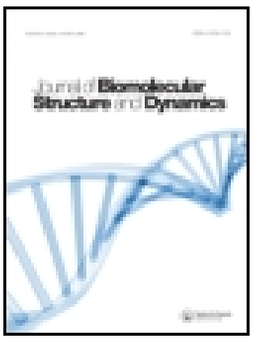

Taylor & Francis
Taylor & Francis Group

Journal of Biomolecular Structure and Dynamics

ISSN: 0739-1102 (Print) 1538-0254 (Online) Journal homepage: http://www.tandfonline.com/loi/tbsd20

Spectroscopic evaluation of synthesized 5β-dihydrocortisol and 5β-dihydrocortisol acetate binding mechanism with human serum albumin and their role in anticancer activity

Monika Kallubai, Srinivasa P Reddy, Shreya Dubey, Dhevalapally B Ramachary & Rajagopal Subramanyam

To cite this article: Monika Kallubai, Srinivasa P Reddy, Shreya Dubey, Dhevalapally B Ramachary & Rajagopal Subramanyam (2018): Spectroscopic evaluation of synthesized 5β-dihydrocortisol and 5β-dihydrocortisol acetate binding mechanism with human serum albumin and their role in anticancer activity, Journal of Biomolecular Structure and Dynamics, DOI: 10.1080/07391102.2018.1433554

To link to this article: https://doi.org/10.1080/07391102.2018.1433554

Accepted author version posted online: 29 Jan 2018.

Publisher: Taylor & Francis

Journal: *Journal of Biomolecular Structure and Dynamics*

DOI: http://doi.org/10.1080/07391102.2018.1433554

Spectroscopic evaluation of synthesized 5β-dihydrocortisol and 5β-dihydrocortisol acetate binding mechanism with human serum albumin and their role in anticancer activity

Monika Kallubai[a] , Srinivasa P Reddy[b] , Shreya Dubey[a] , Dhevalapally B Ramachary[b] & Rajagopal Subramanyam[a]

[a] *Department of Plant Sciences, School of Life Sciences, University of Hyderabad, Hyderabad 500046, India*

[b] *Catalysis Laboratory, School of Chemistry, University of Hyderabad, Hyderabad 500046, India*

*Corresponding author

Rajagopal Subramanyam

Department of Plant Sciences

School of Life Sciences

University of Hyderabad 500 046 India

Tel: +91-40-23134572

Fax: +91-40-23010120

Email:srgsl@uohyd.ernet.in

Abstract

Our study focus on the biological importance of synthesized 5β-dihydrocortisol (Dhc) and 5β-dihydrocortisol acetate (DhcA) molecules, the cytotoxic study was performed on breast cancer cell line (MCF-7) normal human embryonic kidney cell line (HEK293), the IC_{50} values for MCF-7 cells were 28 and 25 μM, respectively, whereas no toxicity in terms of cell viability was observed with HEK293 cell line. Further experiment proved that Dhc and DhcA induced 35.6% and 37.7% early apoptotic cells and 2.5%, 2.9% late apoptotic cells respectively, morphological observation of cell death through TUNEL assay revealed that Dhc and DhcA induced apoptosis in MCF-7 cells. The complexes of HSA–Dhc and HSA–DhcA were observed as static quenching, and the binding constants (K) was $4.7\pm0.03\times10^4\ M^{-1}$ and $3.9\pm0.05\times10^4\ M^{-1}$, and their binding free energies were found to be -6.4 and -6.16 kcal/mol, respectively. The displacement studies confirmed that lidocaine $1.4\pm0.05\times10^4\ M^{-1}$ replaced Dhc, and phenylbutazone $1.5\pm0.05\times10^4\ M^{-1}$ replaced by DhcA, which explains domain I and domain II are the binding sites for Dhc and DhcA. Further, FT-IR, synchronous spectroscopy, and CD results revealed that the secondary structure of HSA was altered in the presence of Dhc and DhcA. Furthermore, the atomic force microscopy and transmission electron microscopy showed that the dimensions like height and molecular size of the HSA–Dhc and HSA–DhcA complex were

larger compared to HSA alone. Detailed analysis through molecular dynamics simulations also supported greater stability of HSA–Dhc and HSA–DhcA complexes, and root-mean-square-fluctuation interpreted the binding site of Dhc as domain IB and domain IIA for DhcA. This information is valuable for further development of steroid derivative with improved pharmacological significance as novel anti-cancer drugs.

Keywords: 5β-dihydrocortisol; Apoptosis; Fluorescence quenching; Molecular docking; Molecular dynamics simulations; Protein conformations

Introduction

Cortisol is a steroid hormone secreted by the adrenal cortex and is an important glucocorticoid in humans. More than 80% of cortisol binds to cortisol-binding globulin (CBG) in normal intact plasma (Perogamvros, Aarons, Miller, Trainer & Ray 2011). However, when CBG is inactivated by heat or absent, then the majority of cortisol associate with albumin. It has been determined *in vitro* that at 37 °C the dissociation constant (K_d) for cortisol binding to albumin in human serum was about 330 and 810 μM (Mendel, Miller, Siiteri & Murai 1990). Cortisol is usually metabolized in the liver to dihydrocortisol, then to tetrahydrocortisol and finally conjugated to glucuronic acid, which enters the circulation and excreted in the urine. Cortisol metabolites, α-dihydrocortisol and β-dihydrocortisol are known to have affinities for both mineralocorticoid and glucocorticoid receptors. Mineralocorticoid hormones regulate electrolyte balance, in mammals, they increase K+ and H+ and decrease Na+ in the urine. The levels of unconjugated dihydrocortisols in urine give the information of either mineralocorticoid act as agonist or antagonist to the renal aldosterone receptor (Marver & Edelman 1978). Glucocorticoids have multi-systemic effects that are essential for survival in times of stress, influencing the regulation of blood pressure, salt and water balance, immune function and

cellular energy metabolism. The consequences of the failure of these responses cause several syndromes leading to morbidity and mortality. The physiological effects of these hormones result from their specific binding to an intracellular receptor protein. Mineralocorticoid receptor and glucocorticoid receptor, in the absence of hormone, are primarily in the cell cytoplasm, once binding the receptor sheds its associated proteins (serum proteins), translocate to the nucleus for transcription of its target genes. Cortisol has a 21-carbon skeleton, modifications to this skeleton and other corticosteroids selectively alter the metabolic consequences varying the degree and duration of activity, and also protein-binding affinity of the resultant compound. In such modifications, the additional fluorination at the C-9 position enhanced both glucocorticoid and mineralocorticoid activity, as in 9α-fluorocortisol, while fludrocortisone acetate is 125-fold more potent than cortisol for mineralocorticoid effect and only 10-fold more for glucocorticoid effect (Genard & Palem-Vliers 1980). In addition to the tri-hydroxyl groups, 16-acetoxy 10-aldehyde groups in drugs showed enhanced binding affinity with human serum albumin (HSA) (Zhou et al. 2015).

Human serum albumin (HSA) plays a fundamental role in the transport of metabolites, drugs and various endogenous ligands, such as fatty acids. It is synthesized in the liver and exported as a single non-glycosylated chain, reaching blood concentration of about 7.0×10^{-4} M (Fasano et al. 2005; Matsuda et al. 2014; Lambrinidis, Vallianatou & Tsantili-Kakoulidou 2015). The unfolding/refolding strategies of HSA with their exogenous/endogenous ligand binding preference are of immense use in therapeutics, as it is the marvelous binder of therapeutic drugs (Varshney et al. 2010). The X-ray crystallographic analysis of HSA reveals its primary structure containing three homologous domains I, II, and III. Further, each domain is constituted by two subdomains A and B, connected by random coils. In a crystal, all six subdomains assemble to

form a heart-shaped molecule (Carter & Ho 1994). Terminal regions of sequential domains contribute to the formation of inter-domain helices linking domain IB to IIA, and IIB to IIIA, respectively (Curry 2002). Most of the aromatic and heterocyclic ligands are bound within two hydrophobic pockets in subdomains IIA and IIIA, which are referred as sites I and II (Sudlow, Birkett & Wade 1975). In our previous work, we have reported that beta-sitosterol, piperine binds in IIA and L-3,4-dihydroxyphenylalanide binds in IIIA domain of HSA (Sudhamalla, Gokara, Ahalawat, Amooru & Subramanyam 2010; Yeggoni & Subramanyam 2014; Yeggoni, Rachamallu, Kallubai & Subramanyam 2015). It can also be able to bind seven equivalents of long-chain fatty acids (FA1-7) in sub-domains IB, IIIA, IIIB, and on the sub-domain interfaces (Fasano et al. 2005). The principle binding region in HSA is located at IIA region of domain II, which play vital role to transport and deliver various drugs to multiple organs of body. Recent reports showed that various compounds like inhibitor STAT3 for abnormally expressed proteins in cancer cells, an organophosphorous herbicide diazinon, anticancer drug [Pt(5,5′-dmbpy)Cl_4 (5,5′-dmbpy is 5,5′-dimethyl-2,2′-bipyridine) complex, and an alkaloid 5-hydroxy-1-methylpiperidin-2-one were interacted in the IIA region of HSA with good binding affinity (Affandi et al. 2016; Jafari et al. 2017; Shahraki, Somaye, Saeidifar, Shiri & Heidari 2017; Yadav, Yeggoni, Devadasu & Subramanyam 2017). The structure of bufadienolides showed strong variations in their binding with HSA, especially 11-OH and 16-OAC groups improved serum albumin binding contributing to their development as anti-tumor agents (Zhou et al. 2015). Even we reported synthesized nefopam analogues and Androstenedione derivatives binding in the domain IB, IIA and domain IIIA regions (Gokara et al. 2017; Nerusu, Reddy, Ramachary & Subramanyam 2017).

Thus, our current study deals with *in vitro* approach of structure-affinity relationship of

synthesized 5β-dihydrocortisol (Dhc) and 5β-dihydrocortisol acetate (DhcA) with HSA, as it is an important determinant to understand the binding mechanism of these compounds. However, the mode of interaction of these compounds with HSA and its role in disease control was not previously reported. Thus our investigation on Dhc and DhcA binding with HSA through cell-based assay, multiple spectroscopic and molecular docking and dynamics simulation studies emphasized the biological importance, nature of the binding sites, the strength and variations in these interactions, as well as the possible conformational changes.

Materials and methods

Synthesis of 5β-Dihydrocortisol and 5β-Dihydrocortisol acetate

General procedure for palladium/charcoal catalyzed hydrogenation of cortisol

The mixture of 5% Pd/C (5 mol%), Hantzsch ester (152 mg, 0.9 mmol) and the cortisol (0.3 mmol) in EtOH (3.0 mL, 0.1 M) was heated to 80 °C for the 6 h. Crude mixture was then passed through a pad of celite. Pure hydrogenated product 5β-dihydrocortisol was obtained by column chromatography (silica gel, mixture of hexane/ethyl acetate) in 86% yield with 72% *de*.

General procedure for organocatalytic hydrogenation of cortisol acetate

(*S*)-(+)-1-(2-Pyrrolidinylmethyl)pyrrolidine (12 mg, 0.075 mmol) and D-camphor sulphonic acid (17 mg, 0.075 mmol) in dry CH_3CN (3.0 mL, 0.1 M) were stirred at rt for 5 min, then added cortisol acetate (0.3 mmol) and stirring was continued at the same temperature for another 5 min. To this, added Hantzsch ester (152 mg, 0.6 mmol) and refluxed for the 72 h. The crude reaction mixture was purified with aqueous work-up followed by column chromatography (silica gel, mixture of hexane/ethyl acetate) in 52% yield with 66% *de* (Ramachary, Sakthidevi & Reddy 2013).

Preparation of stock solutions

Fatty acid-free with above 95% purity HSA was purchased from Sigma-Aldrich, USA. The stock solution (1.5 mM) of HSA was prepared in 0.1 M phosphate buffer at pH 7.4. Dilutions of the HSA stock solutions was made to a final concentration (0.001 mM) in phosphate buffer of pH 7.4 were prepared immediately before use. The molecular weight of 5β-dihydrocortisol and 5β- dihydrocortisol acetate are 364.47 and 406.51 Da, and the purity of molecules are more than 97%, their stock solutions were prepared by dissolving them in small amount of ethanol and then diluting them to (1.0×10^3 M^{-1}) solution. Site-specific markers phenylbutazone, lidocaine, and ibuprofen solutions were also prepared at concentrations 0.001 mM. All other chemicals used for the experiments in our study are of analytical grade purchased from Sigma-Aldrich.

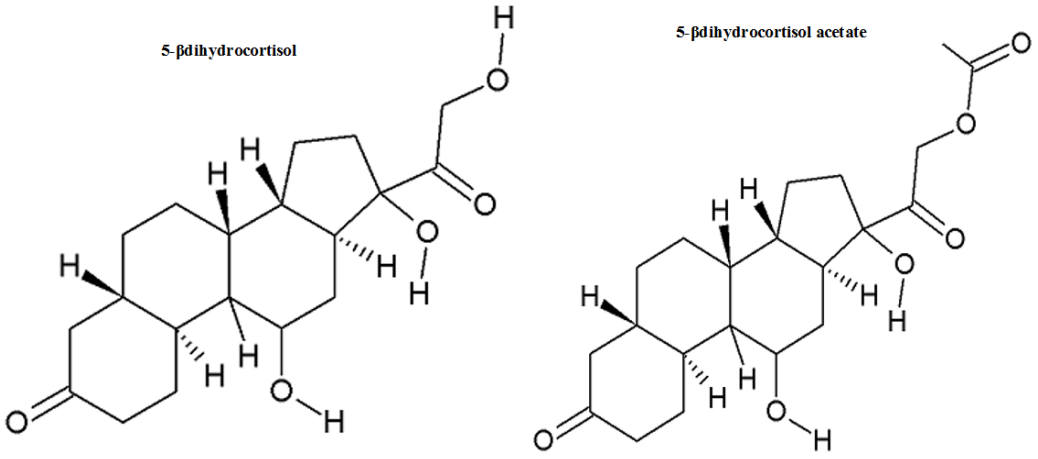

Schematic representation of 5β-dihydrocortisol and 5β-dihydrocortisol acetate

Cell viability assay (MTT assay)

The MCF-7 cells and HEK 293 were procured from the cell repository, National Centre for Cell Science, NCCS complex, Pune. The cytotoxic activity of Dhc and DhcA on MCF-7 and HEK 293 were determined by MTT (3-(4, 5-dimethyl thiazol-2yl)-2, 5-diphenyl tetrazolium bromide) assay. Cells (1×10^5/well) were seeded in 96-well plates and treated with Dhc and DhcA

in increasing concentrations of 20, 40, 60, 80 and 100 µM for 48 h in a final volume of 100 µL. At the end of treatment, 20 µL of MTT (5 mg MTT/ml in PBS) was added, and the cells were incubated for 3-4 h, control was maintained without the drug. About 100 µL of DMSO (solubilizing reagent) was added to each well and mixed well by micropipette. Presence of viable cells was visualized by the development of purple color due to the formation of formazan crystals. Relative cell response was evaluated by measuring the optical density at 570 nm on a microplate reader (µ Quant Bio-tek Instruments, Inc.). Three independent experiments were performed, measurements were performed, and the concentration required for a 50% inhibition of viability (IC_{50}) was determined through standard graph plotted by taking a concentration of the drug in X-axis and percentage inhibition in Y-axis.

Apoptosis assay

The Annexin/PI assay is a widely used approach for studying apoptotic cells. Propidium iodide in conjunction with Annexin V significantly determines the viable, apoptotic and necrotic cells through differences in plasma membrane integrity and permeability. The MCF-7 cells (2 mL) at a density of 5×10^3 were grown in 6 well plate and allowed to attach for 24 h after which cells were treated with half the IC_{50} values of Dhc and DhcA 14 µM, 12.5 µM for 24 h. Then cells were washed twice with 1% phosphate buffer saline, resuspended in Annexin V binding buffer. The cells were centrifuged for 10 min, and supernatants were discarded, again cells were suspended in 100 μL Annexin V binding buffer, incubated in the dark for 15 min. Propidium Iodide (4 μL) diluted in 1x Annexin V binding buffer (1 : 10) was added and allowed to incubate for 15 min in the dark at room temperature. The experiment were done using the Annexin V-FITC detection kit (Sigma, cat. no. APOAF) and the results were analyzed by flow cytometry.

Tunel assay

TUNEL assay uses (terminal deoxynucleotidyl transferase-TdT mediated dUTP nick end-labeling) to label 3'-OH ends of DNA fragments that are generated during the process of apoptosis. The DNA fragmentation was assessed by a commercial kit (In situ Apoptosis Detection Kit #MK500 from TaKaRa), in accordance with the manufacturer's instructions. MCF-7 cells (1×10^6 cells/ml) were exposed to half the IC50 values of Dhc and DhcA obtained from cell viability assay, i.e. 14 and 12.5 μM, a control was maintained without test compounds for 24 h. The cells were fixed with 4% (v/v) methanol-free formaldehyde/PBS solution at 4°C for 25 min and rinsed again with PBS. Subsequently, the cells were permeabilised by immersion in 0.2% Triton X-100 in PBS (pH 7.4) for 5 min, rinsed in PBS and equilibrated with the equilibration buffer for 10 min. Cells were labelled by incubating at 37°C with the TdT (terminal deoxynucleotidyl transferase) incubation buffer for 60 min. The reaction was stopped by immersing the slides in saline sodium citrate for 15 min. Finally, slides were washed with PBS and treated with propidium iodide (10 μg/mL in PBS) for 15 min in dark conditions. Observations were made by using confocal fluorescence scanning microscope (Carl-Zeiss, Germany). The green fluorescent cells is considered as an apoptotic hallmark.

Fluorescence quenching

Fluorescence spectroscopy is a convenient and simple method to study the binding of HSA by small ligands. The fluorescence emission spectra were carried out on a LS-55 spectrofluorimeter (PerkinElmer corporate, USA). The excitation and emission slit widths were set at 5 nm, and the excitation wavelength was 285 nm while emission wavelengths were recorded between 300-500 nm. The HSA concentration (0.001 mM) was kept constant throughout the study, although the Dhc and DhcA varied from 0.001 to 0.01 mM. The incubation time for each concentration of both Dhc and DhcA with HSA was 10 minutes. The experiment

was done for three times and each time identical spectra were observed.

The fluorescence intensity was measured through quenching, where a variety of molecular interactions can occur. Such excited state reactions, molecular rearrangements, energy transfer, ground-state complex formation and collisional quenching is described by the modified Stern-Volmer equation (Liang, Tajmir-Riahi & Subirade 2008).

Molecular displacement

Displacement studies between HSA and Dhc and DhcA in the presence of site-specific markers like lidocaine, phenylbutazone, and ibuprofen for the site I, II and III respectively (Yeggoni et al. 2014), were executed using the fluorescence spectroscopy. The concentration of HSA and the site-specific markers were kept constant (0.001 mM), while the concentration of Dhc and DhcA increased from 0.001 to 0.01 mM. An excitation wavelength of 285 nm was chosen and the fluorescence emission acquired from 300-500 nm. The fluorescence spectra were recorded, and the binding constants of the HSA-site marker-ligand were evaluated.

Synchronous fluorescence spectroscopy

To exploit the induced structural changes in HSA with the addition of Dhc and DhcA, synchronous fluorescence analysis of HSA has been performed. The fixed concentration of HSA 0.001 mM was titrated with increased concentrations of Dhc and DhcA (0.001-0.01 mM). The spectra were recorded from 300 to 450 nm by setting the excitation and emission wavelength interval ($\Delta\lambda$) at 15 and 60 nm.

Atomic force microscopy

Atomic force microscopy was carried out to observe the topological changes of free HSA and HSA–Dhc and HSA–DhcA by NT-MDT Solver scanning probe microscopy. The cantilever (0.3mm) have an Au high reflectivity coating, tip height 14-16μm, force constant (5, 5 N/m) and

the typical imaging resonance frequency was 140 kHz (Yeggoni, Rachamallu & Subramanyam 2016). Samples were prepared as follows: (1) free HSA with 50 μL of 2 μM HSA was added to a glass slide and incubated for 20 min at room temperature before washing with water and (2) Dhc–HSA and DhcA–HSA complexes with free HSA samples were prepared as described in step 1: prior to adding 50 μL of a 10 μM Dhc and DhcA solutions, incubating for 20 min and washed with water then dried under N2 for 5 min, and the samples were imaged from AFM in noncontact mode (Zhang, Gu & Zhang 2014)

Transmission electron microscopy (TEM)

The size and external morphology of HSA and HSA–Dhc and HSA–DhcA complexes in aqueous solution at pH 7.4 were determined by transmission electron microscopy (TEM) using FE1 Tecnai G2S-Twin-200kv. The samples (HSA (0.001mM), HSA (10 μM) + Dhc (50 μM) solution, HSA (0.001M) + DhcA (50 μM) solution) were prepared freshly by placing one preparation drop (5–10 μL) on a carbon coated copper grids, and the sample was dried completely, a piece of filter paper is used to absorb any excess liquid present on the grid. Finally at room temperature, a drop of 2% uranyl acetate negative stain was added before drying and further observed the structure of HSA and HSA–Dhc and HSA–DhcA complexes under TEM (Yeggoni, Rachamallu & Subramanyam 2016).

Molecular docking

Docking experiment was performed using Discovery Studio Modeling 2.1 (Accelrys Inc.) and Autodock 4.2.1. The small molecules Dhc and DhcA (ligands) were constructed using Discovery Studio Modeling 2.1, hydrogens are added, and the ligands were energy minimized before docking runs. The crystal structure of HSA (receptor) PDB ID: 1AO6 was extracted from Protein Data Bank (http://www.rcsb.org/pdb) deleting water (HET atoms) molecules (Sugio,

Kashima, Mochizuki, Noda & Kobayashi 1999). Docking calculations were performed using the standard procedure for rigid protein and a flexible ligand using Autodock 4.2.1 (Morris et al. 2009). The Lamarckian genetic algorithm (LGA) was applied in the docking calculations. All of the torsional bonds of the ligands were free to rotate while HSA was held rigid. Then, the polar hydrogen atoms were added for HSA using the AutoDock tools, and Kollman united partial atom charges (Morris, Goodsell, Huey & Olson 1996), were assigned. A total of 50 independent runs were carried out with a maximum of energy evaluations to 25,000,000 and a population size to 150. A grid box (126×126×126) with a spacing of 0.534 Å was created. Energy grid maps for all possible ligand atom types were generated using Autogrid 4.2.1 before performing the docking. During the docking process, a maximum of 50 conformers was generated in 50 docking runs, and the conformation with the lowest energy was used for further analysis.

Molecular dynamic simulations

The lowest docked conformer of HSA-ligand complexes with binding energy near to the experimental value was selected for MD simulations using GROMACS 4.5.5, with a Gromacs96 54a7 force field (Sudhamalla et al. 2010; Pronk et al. 2013). The topologies of HSA were generated using the Gromacs package directly, whereas ligands (Dhc and DhcA) using the PRODRG2.5 Server (Schuttelkopf & van Aalten 2004), these topologies for HSA-drug were standardized in our previous work (Sudhamalla et al. 2010; Yeggoni et al. 2014; Kallubai, Rachamallu, Yeggoni & Subramanyam 2015). A box was defined which was filled with the simple point charges, Na+ ions (15 in number) were added to make the entire system neutral. Energy minimisation was performed using 100 steps of steepest descent to avoid any kind of bad contacts generated while solvating the system. Subsequently, the temperature was increased gradually from 0 K to 300 K over a 50 ps time span in the constant-NVT ensemble with a time

step of 0.5 fs. This thermalized configuration was utilized to perform long simulation runs in the constant-NPT ensemble. A Nos´e Hoover thermostat with a coupling constant of 0.1 ps was employed to maintain the temperature of the system at 300 K, while a Parrinello–Rahman barostat with a coupling constant of 2 ps was utilized to maintain the system at 1 bar pressure. The LINCS algorithm was utilized to keep all the covalent bonds involving hydrogen atoms (C–H, N–H, and O–H) rigid. A time step of 1 fs was used to integrate the equations of motion for all the production runs. However, simulations to obtain the free energy profiles were carried out with a time step of 2 fs constraining all covalent bond lengths. Partial mesh Ewald algorithm was employed for measuring electrostatic, and van der Waals interactions; the short-range neighbor list cut-off, short-range electrostatic cut-off, and short-range van der Waals cut-off were fixed at 1 nm. The trajectories were generated up to 10-ns. All the simulations were performed on the Linux cluster with 36 nodes (dual Xeon processor) at the Bioinformatics facility of the University of Hyderabad.

Results and discussion

Cytotoxic studies of Dhc and DhcA

Steroidal and nonsteroidal endocrine agents are important in the therapy and control of advanced breast and prostate cancers. For breast cancer, in particular, the presence of specific estrogen binding in fresh biopsy specimens determines which tumors respond to endocrine therapy. Previous results explained that β-sitosterol and dihydrocortisol showed anti-cancer activity in breast cancer cell line (MCF-7) (Zava, Chamness, Horwitz & McGuire 1977; Pradhan et al. 2017). Thus, we selected human breast carcinoma cells (MCF-7) and normal human embryonic kidney cell line (HEK 293) to evaluate the cytotoxicity of synthesized compounds of 5β-dihydrocortisol and 5β-dihydrocortisol acetate using MTT assay. Inhibition of cell viability

was very less in HEK 293 cells, hence both synthesized Dhc and DhcA did not showed any effect on cell cytotoxicity in a concentration-dependent manner (Figure 1(B)). Whereas, MCF-7 cells induced cytotoxicity and the IC50 values for Dhc and DhcA were 28 μM and 25 μM respectively (Figure 1(A)), which are significant value. In another report, acetoxycoumarin drugs showed strong anti-proliferative activity and induced apoptosis in various cancer cell lines such as A549 (lung), ACHN (renal), H727 (lung), MCF-7 (breast) and HL-60 (leukemia). 4-(7-(diethylamino)-4-methyl-2-oxo-2H-chromen-3-yl)phenyl acetate had the highest cytotoxic activity of 48.1 μM (Musa et al. 2011). Thus, our results explain that due to the addition of acetate group in 5β-dihydrocortisol acetate could be more toxic to cancer cells. Thus, Dhc and DhcA are could be the potential therapeutic agents to cure breast cancer.

Apoptosis assay

Apoptosis plays an important role in controlling the cell number and proliferation. Now a days the development of novel drugs able to restore the normal apoptotic pathway represents a new strategy in cancer treatment (Cordeu et al. 2007). In the present work we investigated using half the concentrations of IC_{50} values of Dhc 14 μM and DhcA 12.5 μM obtained from cell viability assay to induce apoptosis in MCF-7 cells. The apoptotic effect was evaluated using Annexin-V-FITC/PI dual staining assay, which can examine phosphatidylserine translocation to the cell surface precedes nuclear breakdown, DNA fragmentation, and the appearance of most apoptosis-associated molecules making Annexin V binding a marker of early stage apoptosis. The data obtained in this study are presented in (Figure 2(A)), as a percentage of early apoptotic cells, late apoptotic cells, and necrotic cells in quadrants. The results showed that 12.5 μM concentration of DhcA induced 37.7%, 2.9% of early and late apoptosis, whereas dhc showed 35.6% and 2.5%. Our results suggest that synthesized molecules Dhc and DhcA are potent

antitumor agents and cause cell apoptosis, 5β-dihydrocortisol acetate induced more percentage of apoptotic cells. Even previous reports showed that other molecules like 1'-Acetoxychavicol acetate induced apoptosis in myeloma cells via different pathways (Ito et al. 2005). Hence, our results suggest that Dhc and DhcA are a strong inhibitor of MCF--7 cells and hence these molecules can be used for further *in vivo* studies for treating breast cancer.

Tunel assay

The pro-apoptotic efficacy of Dhc and DhcA were further verified on MCF-7 cancer cell line by Tunel assay. Fragment DNA has a free 3′-OH group which is a substrate for binding of fluorescein-dUTP provide a better evaluation of DNA damage in cell. As expected, the TUNEL-positive cells were increased after treatment with 14 and 12.5 µM of Dhc and DhcA after 48 h (Figure 2(B) and Figure 2(D)). The significant increase in the green fluorescent cells were observed in the treated sample compared to untreated sample, indicates the apoptotic cells with fragmented DNA and the percentage of TUNEL-positive cells correlated closely with the annexin V-positive cells in Figure 2(B) and 2(D). Thus, the data from both annexin V-PI double staining and TUNEL assay consistently showed that Dhc and DhcA predominantly induced apoptosis in cultured MCF-7 cells.

Analysis of fluorescence emission studies

The intrinsic fluorescence of proteins is derived mainly from tryptophan and tyrosine residues, while the quantum yield of the phenylalanine residue is very low. Due to a variety of molecular interactions, there is a decrease in the fluorescence intensity from the fluorophore which is referred to as fluorescence quenching. The molecular interactions include excited-state reactions, molecular rearrangements, energy transfer, and ground-state complex formation. To understand the binding mechanism, the HSA excitation was fixed at 285 nm and titrated with

different concentrations of both Dhc and DhcA. Fluorescence emission spectra exhibit the fluorescence intensity of HSA which quenched by the addition of Dhc and DhcA in a concentration-dependent manner (0.001 mM-0.010 mM) (Figure 3). The fluorescence intensity is decreased due to the presence of Trp214 in HSA, which is sensitive to the ligand binding. Moreover, the Dhc and DhcA did not interfere with the determination of intrinsic fluorescence as no fluorescence emission observed in the range of 300-500 nm. Therefore, Dhc and DhcA could quench the intrinsic fluorescence of HSA with a maximum emission peak at 360 nm, and there was no shift in fluorescence peak indicates that there could be conjugation or complex formation between ligand and HSA.

Determination of binding constant and binding sites

To understand the fluorescence quenching mode of HSA–Dhc and HSA–DhcA complexes, the quenching data were analyzed using the following equation:

$$F_0 / F = 1 + K_q t_0 [Q] = 1 + K_D [Q] \quad \text{- (1)}$$

Where F and F_o are the fluorescence intensities in the presence and absence of quencher, [Q] is the quencher concentration, and K_D is the Stern-Volmer quenching constant (Kq), which can be written as K_D = kqt0; where kq is the biomolecular quenching rate constant and t_0 is the lifetime of the fluorophore in the absence of quencher is 5.6 ns (Liang et al. 2008). From the above equation, the quenching constant was calculated to be 5.0×10^{13} M^{-1} s^{-1} for Dhc and 5.4×10^{13} M^{-1} s^{-1} for DhcA. Hence, the quenching mechanism is static, as these values are much greater than the maximum collisional quenching constant 2.0×10^{10} M^{-1} s^{-1} (Agudelo et al. 2012). Thus, Dhc and DhcA binding to HSA is a static process. The binding constant (K) and the number of bound complexes to HSA (n) were determined by plotting the fluorescence data using modified Stern-Volmer equation

$$log[(F_0 - F)/F] = logK_s + nlog[Q] \quad - (2)$$

Where n is the number of ligands binding to the protein, K_s is the binding constant, and [Q] is the drug concentration. The dF is $(F_0 - F)$, where F_0 is the initial fluorescence of free HSA and F is fluorescence with different concentrations of Dhc and DhcA. We have plotted a graph log (dF/F) against log[Q]. A graph was plotted with the slope and the intercept that can be correlated with the binding constant and the number of binding sites, respectively. The number of binding sites for Dhc and DhcA is 0.85 and 0.96 indicates that binding of these compounds to HSA would be one to one interaction (S. Figure 1). Also, the binding constant (Figure 3(A) and 3(B)) found to be $K_{Dhc} = 4.7 \pm 0.03 \times 10^4\ M^{-1}$ and $K_{DhcA} = 3.9 \pm 0.05 \times 10^4\ M^{-1}$ indicates the strong binding of Dhc and DhcA with HSA. The binding constants are ranging from 10^3 to 10^5 which is regarded as an appropriate scope for association and dissociation of the drug-protein system (Schiel & Hage 2009).

Free energy changes upon binding of Dhc and DhcA to the protein

Usually, there are four types of non-covalent forces such as hydrogen bonding, van der Waals, hydrophobic and electrostatic interactions which stabilize their binding. In order to understand the binding interactions, the free energy change (ΔG°) can be calculated from the following equation:

$$\Delta G° = -RTlnK \quad -(3)$$

Where, ΔG° is the free energy change, R is the gas constant at room temperature, and K is the binding constant. From the above equation, the free energy change for Dhc and DhcA HSA been calculated and found to be -6.8±0.012 and -5.9±0.035 Kcal/mol at 25°C. Similar results were found in molecular docking of Dhc and DhcA -6.44 and -6.16 Kcal/mol with HSA. Therefore,

these data suggests that the binding between protein and ligand can be stabilized by hydrophobic interaction and hydrogen bond formation. Our previous results published recently were also found similar kind of free energies with, 7-hydroxycoumarin, lupeol and lupeol derivative and coumarin derivatives (Garg et al. 2013; Yeggoni et al. 2014; Kallubai et al. 2015).

Molecular displacement studies

The displacement experiments were conducted with several site-specific drugs such as lidocaine, ibuprofen and phenylbutazone reported to be bind with HSA and are specific in their locations at domain IB, (Hein et al. 2010) site I, (Ghuman et al. 2005) and site II (Yamasaki et al. 2000). The fluorescence intensity was measured after addition of 0.01 mM of site-specific marker to 0.001 mM HSA, later the quenching was measured at the different concentrations of Dhc and DhcA, respectively. The experiment was repeated for all the three site-specific markers, and the binding constants were calculated. Figure 3(C) and 3(D) shows decrease in the value of binding constant for lidocaine $K_{ld+Dhc} = 1.4\pm0.02\times10^4$ in the presence of Dhc compared to HSA–Dhc ($K_{Dhc} = 4.7\pm0.03\times10^4$) alone, whereas, phenylbutazone showed decreased binding constant value of $K_{pb+DhcA} = 1.5\pm0.03\times10^4$ against HSA–DhcA ($K_{Dhc} = 3.9\pm0.05\times10^4$). However, there are no observed changes in their binding constants with other site-specific markers of HSA. Therefore, the binding site of Dhc is domain I and for DhcA is domain II. Even molecular docking studies showed Dhc binding in the IB region and DhcA in the domain IIA region. These two molecules bind to different binding pocket because these molecules have different functional groups like –OH in Dhc and acetate in DhcA.

Change in secondary structure observation through synchronous spectroscopy, FT-IR and circular dichroism

Synchronous spectroscopy

The synchronous fluorescence spectroscopy (SFS) technique was used to study the conformational change of protein. It involves simultaneous scanning of the excitation and emission monochromators of a fluorimeter while maintaining a constant wavelength interval ($\Delta\lambda$) between them. The shift in the position of maximum emission reflects the changes in polarity around the chromophore molecule (Poulli, Chantzos, Mousdis & Georgiou 2009). When $\Delta\lambda$ is fixed at 60 nm and 15 nm, the synchronous fluorescence of HSA is characteristic of tryptophan and tyrosine residues. The concentration of HSA was kept constant 0.001 mM and was progressively titrated with Dhc and DhcA by gradually increasing their concentrations as stated in the fluorescence spectroscopy experiment. This data shows small shifts in the spectra at 15 nm, which express a slight change in conformation of HSA upon binding with Dhc (S. Figure 2(A) and 2(C)). In contrast at 60 nm, the influence of tryptophan residues was not observed. While (S. Figure 2(B)) suggests slight change at 15 nm upon binding of DhcA with HSA indicating a change in microenvironment in the vicinity of tyrosine residues. At 60 nm the maximum emission peak shifted towards higher wavelength, which indicates the stretch of HSA molecule after binding DhcA, thus the polarity around the tryptophan residues decreased, increasing the hydrophobicity (S. Figure 2(D)). Similar results were shown that the microenvironment around the trptophan residues of HSA, became more hydrophobic, after addition of norfloxacin at $\Delta\lambda$=60 nm (Azimi, Emami, Salari & Chamani 2011). The results reveal that the polarity around the tryptophan residues after binding Dhc had no remarkable change, while the fluorescent aromatic residues buried in nonpolar hydrophobic cavities are moved to a more hydrophilic environment in the binding process of DhcA, similar results were showed with Nordihydroguaiaretic acid binding with Human serum albumin and Nintedanib binding with Bovine serum albumin (Nusrat et al. 2016; Abdelhameed et al. 2017).

Fourier transform infrared spectroscopy (FT-IR)

IR spectroscopy is used as a powerful tool for investigating the secondary structure of proteins. Infrared spectra of a protein exhibit a number of so-called amide bands, which are sensitive to the secondary structure of proteins**.** The amides I and II peak occur in the region of 1600–1700 cm^{-1} (mainly C=O stretch) and 1500–1600 cm^{-1} (C-N stretch coupled with N-H bending mode) have been widely used, and both are related to the secondary structure of the protein (Rahmelow & Hubner 1996). The FT–IR spectrum of free HSA and the difference in the spectra after binding with Dhc and DhcA were shown in (S. Figure 3). The spectral changes showing the amide I band shifted from 1649±0.5 to 1634±0.6 cm^{-1} and 1648±0.2, while the amide II peak was shifted from 1544±0.7 to 1529±0.9 cm^{-1} and 1514±0.5 binding with Dhc and DhcA to HSA (S. Figure 3(A) and 3(B)). These results indicated that Dhc interacted both with the C=O and C-N groups in the protein polypeptides. The earlier report shows that both hydrophilic and hydrophobic interactions occur for Chol and DOPE-HSA adducts (Charbonneau, Beauregard & Tajmir-Riahi 2009). The spectra indicates that when DhcA enters the hydrophobic binding cavities (subdomain IIA or IIIA) via hydrophobic interactions, the oxygen atom and hydroxyl group of DhcA can form hydrogen bonding with the C=O and C–N groups of the main polypeptide in HSA, resulting in rearrangement of the polypeptide carbonyl hydrogen-bonding network and reduction in the α-helical structure of the protein (Pu, Jiang, Chen & Wang 2014). Thus HSA–Dhc and HSA–DhcA complex formation showed considerable changes in the rigidity of protein molecule, which affects secondary structure of HSA and this result supports with the molecular dynamics simulations data.

Protein conformational changes observed from Circular dichroism

Further to get more information on the structural changes of HSA upon addition of Dhc

and DhcA, the CD spectroscopy is one of the best methods for examining the conformational changes of protein. The CD spectra of HSA exhibit two negative bands in the far-ultraviolet region at 208 and 220 nm, these peaks attributed to n→π* transition for the peptide bond of α-helix (Greenfield 1996).

The CD spectra of free HSA (0.001 mM) and in the presence of Dhc and DhcA are given in (Figure 4(A) and 4(B)). The decrease in intensity of HSA at 208 and 220 nm as the concentration increases of Dhc and DhcA. This indicated the considerable changes in the protein secondary structure upon binding of Dhc and DhcA. Specifically, the loss of α-helical stability, which might be the result of the formation of a complex between the protein and Dhc, DhcA. Here, CDDN web-based software was used to calculate the secondary structural elements. In free HSA, the secondary structure consisted of 58.4±0.5% of α-helices, 22.8±1.2% of β-sheets and 18.8±1.5% random coil, respectively. However, with an increase of 0.001 and 0.002 mM of Dhc, there was a significant change in α-helices i.e. 58±0.3% and 56.3±0.5%, and the percentage change in secondary structural elements is given in Table 1. The change in protein conformation could be a partial unfolding of the protein. After addition of 0.001 and 0.002 mM of DhcA, the α-helical stability was decreased to 56.2±0.8% and 53±0.3% respectively, and this data is in agreement with synchronous fluorescence. We also checked for the thermal stability of Dhc and DhcA bound HSA, and the stability of protein was up to 65° C (data not shown), and the results were similar to the HSA-lupeol complex (Kallubai et al. 2015), indicates that HSA-Dhc/DhcA complexes are stable. Therefore, Dhc and DhcA were bound to the amino acid residues of HSA by non-covalent interactions, which destroyed the hydrogen bonding network, causing the partial unfolding of the polypeptide of HSA in turn change in secondary structure of HSA (Kang et al. 2004). Hence, the HSA–Dhc/DhcA complexes are stable.

Atomic force microscopy

AFM experiment was performed to understand the topographical changes of free HSA upon addition of Dhc and DhcA. Figure 5, displays the results for the free HSA and its HSA–Dhc, HSA–DhcA complexes. Figure 5(A) and 5(D) shows the even distribution of free HSA on the glass slide with the mean height of the individual HSA of 16.00±3.0 nm. After addition of 10 μM of Dhc, the HSA molecule became swollen reaching the mean height of molecule to 20.0±5.0 nm (Figure 5(B) and 5(E)) depicts the formation of HSA–Dhc complex. The same concentration of DhcA added to HSA showed the mean height of 30.0±2.0 nm (Figure 5(C) and 5(F)) and this could be explained that upon binding DhcA perturbs more structural conformation than Dhc. The different shapes and size distributions point towards distinctly different forms of the morphology of free HSA, HSA–Dhc and HSA–DhcA complex and also differential conformation. Thus, the shape of HSA–Dhc complex is different and varied from HSA–DhcA complex, even the mean height also conclude that HSA–DhcA complex is more than HSA–Dhc complex. These results explain that after addition of DhcA, the HSA molecule reduced its surface area of contact with water by molecular aggregation, which further reveal the microenvironment surrounding the HSA became more hydrophobic after interacting with DhcA. Similar results were obtained for HSA-corilagin, HSA–S^4TdR and HSA–patulin complexes (Yuqin et al. 2014; Zhang et al. 2014; Yeggoni et al. 2016). The increase in size of the protein is an indication of formation complexes of HSA–Dhc/DhcA.

Transmission electron microscopy

Further, we also confirmed the binding of th molecule with HSA using an electron microscope and can provide information about the size and morphological changes to understand the dynamic properties of molecules. Hence, the electron microscopy is one of the best tools to

see the protein topology upon binding of Dhc and DhcA with HSA. Figure 6(A) shows the evenly distributed spherical shape particles of free HSA with mean particle diameter of 48.3±2.5 nm. Figure 6(B) and 6(C) shows the HSA–Dhc complex with a diameter of 51.2±3.6 nm, while HSA–DhcA complex with 57.4±4 nm diameter. The results of TEM images explain that the morphology or shape of free HSA, HSA–Dhc and HSA–DhcA are different. HSA–DhcA complex showed large variation in diameter compared to HSA–Dhc complex; this may be probably due to conformational changes within the globular structure of HSA after binding with DhcA. The morphological difference of HSA upon addition of Dhc are attributed to slight structural changes. While more structural changes would have happened upon DhcA complexation. Formation of large aggregates is chracterized by a decrease of helical structure and slight increase in the β-sheet. Hydrogen bonding from those polar groups probably takes place in the aqueous environment. The TEM results are very well supported by the AFM data where we can see a broad aggregate for HSA–DhcA complex. The AFM and TEM data (more surface changes on protein) are in agreement with cell line data that DhcA is showing better cytotoxicity activity where it act again breast cancer cell lines.

Molecular docking studies

Molecular docking gives the detailed picture of the binding site of drugs, its position, and orientations of the protein. This information is crucial as it explains the relationship between molecular properties of complexes. In our previous studies, we analyzed docking studies on different PDB structures of HSA with PDB ID: 1AO6, 2BXC, 1BM0 and obtained similar docking energies (Kallubai et al. 2015). Assuming that docking on different crystal structures of HSA gives no difference in binding sites as we selected PDB ID: 1AO6 as a template structure to identify the possible binding sites of Dhc and DhcA. Out of 50 docked conformations, the

highest affinity site regarding docked energy for Dhc and DhcA is domain IB and domain IIA. The docked energies are -6.44 k.cal/mol and -6.18 K.cal/mol, which correlates with the free energies obtained from experimental data of fluorescence emission. Molecular displacement studies revealing that the Dhc replaced the lidocaine binding site domain IB and DhcA with phenylbutazone of domain IIA (Figure 3(C) and 3(D)). The binding site of Dhc obtained from docking results showed four hydrogen bonds, three OH- groups interacting with Pro110, Leu112 and Leu115, while carbonyl oxygen with His146 with bond distances 2.116, 2.206, 1.869 and 2.145 Å, all these residues lie in domain IB (Figure 7(C)). Another reports supports our results that tamoxifen an antitumor drug for the treatment of breast cancer and its metabolite 4-hydroxytamoxifen also showed stronger interaction in the vicinity of domain I region of HSA via hydrophobic and hydrogen-bonds formation (Bourassa, Thomas & Tajmir Riahi 2016). DhcA was located between subdomain IIA and IIIA of HSA (Figure 7(D) and 7(E)), during the interaction with the residues two hydrogen bonds were established between C=O of acetate group with the residues Trp214, Arg218 with bond distance 1.973 and 1.995 Å, while one –OH group showed hydrogen bond with polar amino acid residue Cys448 present in domain IIIA with bond distance 1.82 Å (Figure 7(F)). The same type of results was observed with HSA–phloretin complex, which showed binding site in between domain IIA and IIIA (Barreca et al. 2016). There is no surprise that Dhc and DhcA binding to two different domains and previously similar type of hormone, ie., thyroid hormone thyroxine also showed primary binding site as the site I and thyroxine di iodophenol ring accommodated in site II (Petersen, Ha, Harohalli, Park & Bhagavan 1997). This explains from our results that these two molecules are binding in different binding pockets because DhcA exhibits more conformational change, increase of topology of electron micrographs and increase size in AFM picture. Bufotalin and cinobufagin are the

compounds belongs to bufadienolides had 16-OAc and 21-O groups, 16-acetyl group of bufotalin showed a stable H-bond interaction in the site I of HSA and also 16-OAc of cinobufagin via H-bond interacted with polar residue of Arg222 in the site I of HSA (Zhou et al. 2015). The addition of different groups like acetylation at C21 position of aldosterone, 9α-fluorocortisol and dihydrocortisol showed an increase of ΔG, negativity, indicating a weaker hydrogen bonding to the receptor of the acetylated side chain (Genard & Palem-Vliers 1983). By the above observations, we can conclude that the interaction between DhcA and HSA is not exclusively hydrophobic in nature but also involves polar interactions. Thus the hydrophobic and hydrogen bond interactions play an important role in stabilizing the HSA–Dhc/DhcA complexes. The results obtained by synchronous fluorescence spectroscopy, and FT-IR also provide experimental evidence for the interactions obtained from molecular docking studies.

Molecular dynamics simulation studies

Molecular dynamics simulations (MDS) is useful for filling in the details, where experimental methods cannot, especially identification of cryptic or allosteric binding sites and protein folding. A complete understanding of atomic energies and molecular mechanism of binding is unattainable using experimental techniques as macromolecular motions after ligand binding are microscopic events that take place in mere millionths of a second. To evaluate the structural stability of the HSA–Dhc and HSA–DhcA complexes, the properties were examined by means of the radius of gyration (Rg), root mean square deviation (RMSD) and root mean square fluctuation (RMSF) of the protein. The radius of gyration (Rg) of a protein is a measure of its compactness during the simulation. As in Figure 8(A), the HSA alone showed some fluctuations at 2000 ps, later achieved equilibration around 4000 ps, in our previous report we

have showed free HSA became stable after 2000 ps (Sudhamalla et al. 2010), whereas HSA–Dhc complex showed some disturbance in compactness of 2.55 to 2.62 nm at 4000ps but during the simulations, especially after 8000 ps, there is an overlap. Whereas the HSA–DhcA complex compactness is 2.54±0.3 nm lower (Figure 9(A)) comparative to HSA–Dhc complex 2.58±0.1 nm, we may assume that upon binding of Dhc and DhcA molecules the protein-ligand undergo more conformational changes. The variations of RMSD values regarding HSA alone and HSA–Dhc and HSA–DhcA complex were plotted from 0 to 10 ns and are shown in Figure 8(B) and 9(B). The analysis of RMSD indicated both systems (HSA and HSA–Dhc and HSA–DhcA complex) reached stability and balance after 3 ns simulation time till the end of 10 ns MD simulation time, indicating that the molecular systems were well behaved thereafter. The calculated average RMSD values of HSA, HSA–Dhc and HSA–DhcA complex were 0.4± 0.5 nm and 0.35± 0.2 nm, 0.32±0.70 nm respectively, at which point they achieved an equilibrium state. In addition, the RMSF of all amino acid residues of HSA and in HSA–Dhc, HSA–DhcA complex were examined to reveal the flexibility of residues of HSA. Figure 8(C) shows a plot of RMSF of HSA and HSA–Dhc complex against residue number. These results indicated that residues 100-150 (Pro110, Leu112, and Leu115) located in the domain I seem to be more rigid due to the HSA–Dhc complex formation. Whereas, in Figure 9(C) the HSA–DhcA complex is showing rigidity of residues 200-230 (Trp214, Arg218, Cys448), which explains that the DhcA is binding in domain IIA. Thus, the fluctuations of the residues all through 10 ns at the binding sites clearly illustrated that Dhc bound to HSA in domain I, and DhcA bound in domain II. Thus the Dhc and DhcA are stable in the domain IB and IIA, which corroborates with all the spectroscopic results explained above. Hence, MDS results shows that HSA–Dhc and HSA–DhcA are formed stable complexes. Further, these compounds could be used for further studies

to understand the potent anti-cancer activity particularly for breast cancer.

Conclusions

The synthesized steroid compounds of Dhc and DhcA interaction with HSA was studied here. The results obtained from the fluorescence spectroscopy suggested that Dhc and DhcA can bind to HSA through static quenching mechanism and the binding constant of the HSA–Dhc and HSA–DhcA complexes was calculated to be $4.7\pm0.03\times10^4\ M^{-1}$ and $3.9\pm0.05\times10^4\ M^{-1}$, respectively. Additionally, molecular displacement experiments proved that the probable binding site for Dhc is domain I, while for DhcA is site I. Even synchronous fluorescence data showed spectral changes at λ15 nm for Dhc, a clear indication of involving tyrosine residues around binding site of Dhc, and spectral changes at λ60 nm for DhcA proves that tryptophan residue is among the one in the binding cavity. From the FT-IR spectroscopy and CD showed results emphasized the conformational changes occurred in the HSA. Further, AFM and TEM results showed that Dhc and DhcA after binding to HSA noticed that there is an increase in the height of surface topology and molecular size. Furthermore, the binding mode was also characterized by a molecular docking and molecular dynamics simulations, which indicated that Dhc could bind in the domain IB via hydrophobic interaction, while DhcA binds in the site I i.e domain IIA via hydrophobic and hydrophilic interactions. All of the experimental and computational data reveal that Dhc and DhcA, through binding to HSA, can be effectively transported and distributed in the blood. Additionally, the cytotoxic studies of Dhc and DhcA reveal that the DhcA showed better inhibitory activity against human breast cancer cells (MCF-7 cancer cell line) than Dhc indicates these compounds are acting against breast cancer. In addition, it was found that Dhc and DhcA induced apoptosis in MCF-7, particularly DhcA exhibited strong anticancer activity in

inhibiting the cells at lower concentration and also increasing the percentage of early and late apoptotic cells. Hence, these results are pivotal in understanding of protein structure-function relationships which in turn gives an important information in drug discovery.

Acknowledgements

We thank BIF, for Bioinformatics facilities and also acknowledge the AFM facility provided by School of Chemistry, TEM and Flow cytometer facility provided under DST-Centre for Nanotechnology, University of Hyderabad.

Funding

This work was supported by Science and Engineering Research Board (SB/EMEQ-064/2014 dated **14-07-2015** and DST-FIST), UGC-SAP and UPE-2 University of Hyderabad. MK acknowledge UGC (Dr. D. S. Kothari Fellowship) for providing financial support.

References

Abdelhameed, A. S., Nusrat, S., Paliwal, S., Zaman, M., Zaidi, N. & Khan, R. H. (2017). A multitechnique approach to probe the interaction of a therapeutic tyrosine kinase inhibitor nintedanib and bovine serum albumin. *Preparative Biochemistry and Biotechnology*, 1-9, doi.10.1080/10826068.2016.1275014.

Affandi, M, I. S., Lee, W. Q., Feroz, S. R., Mohamad, S. B. & Tayyab, S. (2016). Interaction of stattic, a STAT3 inhibitor with human serum albumin: spectroscopic and computational study. *Journal of Biomolecular Structure and Dynamics*, 1-10, doi.10.1080/07391102.2016.1264887.

Agudelo, D., Bourassa, P., Bruneau, J., Berube, G., Asselin, E. & Tajmir-Riahi, H. A. (2012). Probing the binding sites of antibiotic drugs doxorubicin and N-(trifluoroacetyl) doxorubicin with human and bovine serum albumins. *PLoS One 7*, e43814, doi.org/10.1371/journal.pone.0043814.

Azimi, O., Emami, Z., Salari, H. & Chamani, J. (2011). Probing the interaction of human serum albumin with norfloxacin in the presence of high-frequency electromagnetic fields: Fluorescence spectroscopy and circular dichroism investigations. *Molecules, 16*, 9792-9818,

doi:10.3390/molecules16129792.

Barreca, D., Laganà, G., Toscano, G., Calandra, P., Kiselev, M. A., Lombardo, D. & Bellocco, E. (2016). The interaction and binding of flavonoids to human serum albumin modify its conformation, stability and resistance against aggregation and oxidative injuries. *Biochimica et Biophysica Acta (BBA)-General Subjects*, doi.org/10.1016/j.bbagen.2016.03.014.

Bourassa, P., Thomas, T. & Tajmir Riahi, H. (2016). A Short Review on the Delivery of Breast Anticancer Drug Tamoxifen and its Metabolites by Serum Proteins. *Journal of Nanomedicine Research, 4*, 00080.

Carter, D. C. & Ho, J. X. (1994). Structure of serum albumin. *Advances in Protein Chemi*stry *45*, 153-203, doi.org/10.1016/S0065-3233(08)60640-3.

Charbonneau, D., Beauregard, M. & Tajmir-Riahi, H. A. (2009). Structural analysis of human serum albumin complexes with cationic lipids. *Journal of Physical Chemistry B, 113*, 1777-1784, **doi.**10.1021/jp8092012.

Cordeu, L., Cubedo, E., Bandrés, E., Rebollo, A., Sáenz, X., Chozas, H., Domínguez, M. V., Echeverría, M., Mendivil, B. & Sanmartin, C. (2007). Biological profile of new apoptotic agents based on 2, 4-pyrido [2, 3-d] pyrimidine derivatives. *Bioorganic & medicinal chemistry, 15*, 1659-1669, doi.org/10.1016/j.bmc.2006.12.010.

Curry, S. (2002). Beyond expansion: structural studies on the transport roles of human serum albumin. *Vox Sanguinis, 83,* 315-319, doi.10.1111/j.1423-0410.2002.tb05326.

Fasano, M., Curry, S., Terreno, E., Galliano, M., Fanali, G., Narciso, P., Notari, S. & Ascenzi, P. (2005). The extraordinary ligand binding properties of human serum albumin. *IUBMB Life 57*, 787-796, doi. 10.1080/15216540500404093.

Garg, A., Manidhar, D. M., Gokara, M., Malleda, C., Suresh Reddy, C. & Subramanyam, R. (2013). Elucidation of the binding mechanism of coumarin derivatives with human serum albumin. *PLoS One, 8*, e63805, doi.10.1371/journal.pone.0063805.

Genard, P. & Palem-Vliers, M. (1980). Structure-activity relationships for agonistic and antagonistic mineralocorticoids. *Journal of steroid biochemistry, 13*, 1299-1305, doi.10.1016/0022-4731(80)90090-4.

Genard, P. & Palem-Vliers, M. (1983). Role of hydrophobic effects and polar groups in steroid-mineralocorticoid receptor interactions. *Journal of steroid biochemistry*, *19*, 1639-1645, doi.org/10.1016/0022-4731(83)90383-7.

Ghuman, J., Zunszain, P. A., Petitpas, I., Bhattacharya, A. A., Otagiri, M. & Curry, S. (2005). Structural basis of the drug-binding specificity of human serum albumin. *Journal of Molecular Biology, 353*, 38-52, doi.10.1016/j.jmb.2005.07.075.

Gokara, M., Narayana, V. V., Sadarangani, V., Chowdhury, S. R., Varkala, S., Ramachary, D. B. & Subramanyam, R. (2017). Unravelling the binding mechanism and protein stability of human serum albumin while interacting with nefopam analogues: a biophysical and insilico approach. *Journal of Biomolecular Structure and Dynamics, 35*, 2280-2292, doi.10.1080/07391102.2016.1216895.

Greenfield, N. J. (1996). Methods to estimate the conformation of proteins and polypeptides from circular dichroism data. *Anal Biochemisty, 235*, 1-10, doi.10.1006/abio.1996.0084.

Hein, K. L., Kragh-Hansen, U., Morth, J. P., Jeppesen, M. D., Otzen, D., Moller, J. V. & Nissen, P. (2010).

Crystallographic analysis reveals a unique lidocaine binding site on human serum albumin. *Journal of Structural Biology*, *171*, 353-360, doi.10.1016/j.jsb.2010.03.014.

Ito, K., Nakazato, T., Murakami, A., Ohigashi, H., Ikeda, Y. & Kizaki, M. (2005). 1′-Acetoxychavicol acetate induces apoptosis of myeloma cells via induction of TRAIL. *Biochemical and biophysical research communications, 338*, 1702-1710, doi.10.1016/j.bbrc.2005.10.153.

Jafari, F., Samadi, S., Nowroozi, A., Sadrjavadi, K., Moradi, S., Ashrafi-Kooshk, M. R. & Shahlaei, M. (2017). Experimental and Computational studies on the Binding of Diazinon to Human Serum Albumin. *Journal of Biomolecular Structure and Dynamics*, doi.10.1080/07391102.2017.1329096.

Kallubai, M., Rachamallu, A., Yeggoni, D. P. & Subramanyam, R. (2015). Comparative binding mechanism of lupeol compounds with plasma proteins and its pharmacological importance. *Molecular Biosystems, 11*, 1172-1183, doi.10.1039/C4MB00635F.

Kang, J., Liu, Y., Xie, M. X., Li, S., Jiang, M. & Wang, Y. D. (2004). Interactions of human serum albumin with chlorogenic acid and ferulic acid. *Biochimica et Biophysica Acta 1674*, 205-214, doi.10.1016/j.bbagen.2004.06.021.

Lambrinidis, G., Vallianatou, T. & Tsantili-Kakoulidou, A. (2015). In vitro, in silico and integrated strategies for the estimation of plasma protein binding. A review. *Advanced drug delivery reviews, 86*, 27-45, doi.10.1016/j.addr.2015.03.011.

Liang, L., Tajmir-Riahi, H. A. & Subirade, M. (2008). Interaction of beta-lactoglobulin with resveratrol and its biological implications. *Biomacromolecules, 9*, 50-56, **doi.**10.1021/bm700728k.

Marver, D. & Edelman, I. S. (1978). Dihydrocortisol: a potential mineralocorticoid. *Journal of Steroid Biochemistry*, *9*, 1-7, doi.10.1016/0022-4731(78)90093-6.

Matsuda, R., Bi, C., Anguizola, J., Sobansky, M., Rodriguez, E., Badilla, J. V., Zheng, X., Hage, B. & Hage, D. S. (2014). Studies of metabolite–protein interactions: a review. *Journal of Chromatography B*, *966*, 48-58, doi.10.1016/j.jchromb.2013.11.043.

Mendel, C., Miller, M., Siiteri, P. & Murai, J. (1990). Rates of dissociation of steroid and thyroid hormones from human serum albumin. *Journal of steroid biochemistry and molecular biology, 37*, 245-250, doi.10.1016/0960-0760(90)90333-G.

Morris, G. M., Goodsell, D. S., Huey, R. & Olson, A. J. (1996). Distributed automated docking of flexible ligands to proteins: parallel applications of AutoDock 2.4. *Journal of Computer Aided Molecular Design, 10*, 293-304.

Morris, G. M., Huey, R., Lindstrom, W., Sanner, M. F., Belew, R. K., Goodsell, D. S. & Olson, A. J. (2009). AutoDock4 and AutoDockTools4: Automated docking with selective receptor flexibility. *Journal of Computational Chem*istry, *30*, 2785-2791, doi.10.1002/jcc.21256.

Musa, M. A., Badisa, V. L., Latinwo, L. M., Cooperwood, J., Sinclair, A. & Abdullah, A. (2011). Cytotoxic activity of new acetoxycoumarin derivatives in cancer cell lines. *Anticancer Research, 31*, 2017-2022.

Nerusu, A., Reddy, P. S., Ramachary, D. B. & Subramanyam, R. (2017). Unraveling the Stability of Plasma Proteins upon Interaction of Synthesized Androstenedione and Its Derivatives□ A Biophysical and Computational Approach. *ACS Omega, 2*, 6514-6524, **doi.**10.1021/acsomega.7b00577.

Nusrat, S., Siddiqi, M. K., Zaman, M., Zaidi, N., Ajmal, M. R., Alam, P., Qadeer, A., Abdelhameed, A. S. & Khan, R. H. (2016). A comprehensive spectroscopic and computational investigation to probe the interaction of antineoplastic drug nordihydroguaiaretic acid with serum albumins. *PLoS One, 11*, e0158833, doi.10.1371/journal.pone.0158833.

Perogamvros, I., Aarons, L., Miller, A. G., Trainer, P. J. & Ray, D. W. (2011). Corticosteroid-binding globulin regulates cortisol pharmacokinetics. *Clinical Endocrinology, 74*, 30-36, doi.10/1111.j.1365-2265.2010.03897.x

Petersen, C. E., Ha, C. E., Harohalli, K., Park, D. & Bhagavan, N. V. (1997). Mutagenesis studies of thyroxine binding to human serum albumin define an important structural characteristic of

subdomain 2A. *Biochemistry, 36*, 7012-7017, **doi.**10.1021/bi970225v.

Poulli, K. I., Chantzos, N. V., Mousdis, G. A. & Georgiou, C. A. (2009). Synchronous fluorescence spectroscopy: tool for monitoring thermally stressed edible oils. *Journal of Agricutural andFood Chemistry 57*, 8194-8201, **doi.**10.1021/jf902758d.

Pradhan, Madhura, Suri, C., Choudhary, S., Naik, P. K. & Lopus, M. (2017). Elucidation of the anticancer potential and tubulin isotype-specific interactions of β-sitosterol. *Journal of Biomolecular Structure and Dynamics*, 1-14, doi.10.1080/07391102.2016.1271749.

Pronk, S., Pall, S., Schulz, R., Larsson, P., Bjelkmar, P., Apostolov, R., Shirts, M. R., Smith, J. C., Kasson, P. M., van der Spoel, D., Hess, B. & Lindahl, E. (2013). GROMACS 4.5: a high-throughput and highly parallel open source molecular simulation toolkit. *Bioinformatics, 29*, 845-854, doi.10.1093/bioinformatics/btt055.

Pu, H., Jiang, H., Chen, R. & Wang, H. (2014). Studies on the interaction between vincamine and human serum albumin: a spectroscopic approach. *Luminescence, 29*, 471-479, doi.10.1002/bio.2572.

Rahmelow, K. & Hubner, W. (1996). Secondary structure determination of proteins in aqueous solution by infrared spectroscopy: a comparison of multivariate data analysis methods. *Anal Biochemistry, 241*, 5-13, doi.org/10.1006/abio.1996.0369.

Ramachary, D. B., Sakthidevi, R. & Reddy, P. S. (2013). Direct organocatalytic stereoselective transfer hydrogenation of conjugated olefins of steroids. *RSC Advances, 3*, 13497-13506, doi. 10.1039/C3RA41519H.

Schiel, J. E. & Hage, D. S. (2009). Kinetic studies of biological interactions by affinity chromatography. *Journal of separation science*, *32*, 1507-1522, doi.10.1002/jssc.200800685.

Schuttelkopf, A. W. & van Aalten, D. M. (2004). PRODRG: a tool for high-throughput crystallography of protein-ligand complexes. *Acta Crystallographica D Biological Crystallography, 60*, 1355-1363, doi.10.1107/S0907444904011679.

Shahraki, Somaye, Saeidifar, M., Shiri, F. & Heidari, A. (2017). Assessment of the interaction procedure between Pt (IV) prodrug [Pt (5, 5′-dmbpy) Cl4 and human serum albumin: Combination of spectroscopic and molecular modeling technique. *Journal of Biomolecular Structure and Dynamics, 35*, 3098-3106, doi.org/10.1080/07391102.2016.1243074.

Sudhamalla, B., Gokara, M., Ahalawat, N., Amooru, D. G. & Subramanyam, R. (2010). Molecular dynamics simulation and binding studies of beta-sitosterol with human serum albumin and its biological relevance. *Journal of Physical Chemistry B, 114*, 9054-9062, **doi.**10.1021/jp102730p.

Sudlow, G., Birkett, D. J. & Wade, D. N. (1975). The characterization of two specific drug binding sites on human serum albumin. *Molecular Pharmacology, 11*, 824-832.

Sugio, S., Kashima, A., Mochizuki, S., Noda, M. & Kobayashi, K. (1999). Crystal structure of human serum albumin at 2.5 A resolution. *Protein Eng*neering, *12*, 439-446, doi.10.1093/protein/12.6.439.

Varshney, A., Sen, P., Ahmad, E., Rehan, M., Subbarao, N. & Khan, R. H. (2010). Ligand binding strategies of human serum albumin: how can the cargo be utilized? *Chirality, 22*, 77-87, doi. 10.1002/chir.20709.

Yadav, S. A., Yeggoni, D. P., Devadasu, E. & Subramanyam, R. (2017). Molecular binding mechanism of 5-hydroxy-1-methylpiperidin-2-one with human serum albumin. *Journal of Biomolecular Structure and Dynamics*, doi.10.1080/07391102.2017.1300106.

Yamasaki, K., Rahman, M. H., Tsutsumi, Y., Maruyama, T., Ahmed, S., Kragh-Hansen, U. & Otagiri, M. (2000). Circular dichroism simulation shows a site-II-to-site-I displacement of human serum albumin-bound diclofenac by ibuprofen. *AAPS PharmSciTech*, *1*, E12.

Yeggoni, D. P., Gokara, M., Manidhar, D. M., Rachamallu, A., Nakka, S., Reddy, C. S. & Subramanyam, R. (2014). Binding and molecular dynamics studies of 7-hydroxycoumarin derivatives with human serum albumin and its pharmacological importance. *Moleular Pharmaceutics, 11*, 1117-1131, doi.10.1021/mp500051f.

Yeggoni, D. P., Rachamallu, A., Kallubai, M. & Subramanyam, R. (2015). Cytotoxicity and comparative binding mechanism of piperine with human serum albumin and alpha-1-acid glycoprotein. *Journal of Biomolecular Structure Dynamics, 33*, 1336-1351, doi.10.1080/07391102.2014.947326.

Yeggoni, D. P., Rachamallu, A. & Subramanyam, R. (2016). A comparative binding mechanism between human serum albumin and α-1-acid glycoprotein with corilagin: biophysical and computational approach. *RSC Advances, 6*, 40225-40237, doi.10.1039/C6RA06837E.

Yeggoni, D. P., Rachamallu, A. & Subramanyam, R. (2016). Protein stability, conformational change and binding mechanism of human serum albumin upon binding of embelin and its role in disease control. *Journal of Photochemistry Photobiology B, 160,* 248-259, doi.10.1016/j.jphotobiol.2016.04.012.

Yeggoni, D. P. & Subramanyam, R. (2014). Binding studies of l-3, 4-dihydroxyphenylalanine with human serumalbumin. *Molecular Biosystems, 10*, 3101-3110, doi.10.1039/C4MB00408F.

Yuqin, L., Guirong, Y., Zhen, Y., Caihong, L., Baoxiu, J., Jiao, C. & Yurong, G. (2014). Investigation of the interaction between patulin and human serum albumin by a spectroscopic method, atomic force microscopy, and molecular modeling. *Biomed Research International,* 734850, doi.10.1155/2014/734850.

Zava, D. T., Chamness, G. C., Horwitz, K. B. & McGuire, W. L. (1977). Human breast cancer: biologically active estrogen receptor in the absence of estrogen? *Science, 196*, 663-664, doi. 10.1126/science.193182.

Zhang, J., Gu, H. & Zhang, X. (2014). Exploring the binding of 4-thiothymidine with human serum albumin by spectroscopy, atomic force microscopy, and molecular modeling methods. *Carbohydrate Research, 384*, 102-111, doi.org/10.1016/j.carres.2013.11.018.

Zhou, J., Lu, G., Wang, H., Zhang, J., Duan, J., Ma, H. & Wu, Q. (2015). Molecular structure-affinity relationship of bufadienolides and human serum albumin in vitro and molecular docking analysis. *PLoS One, 10*, e0126669, doi.org/10.1371/journal.pone.0126669.

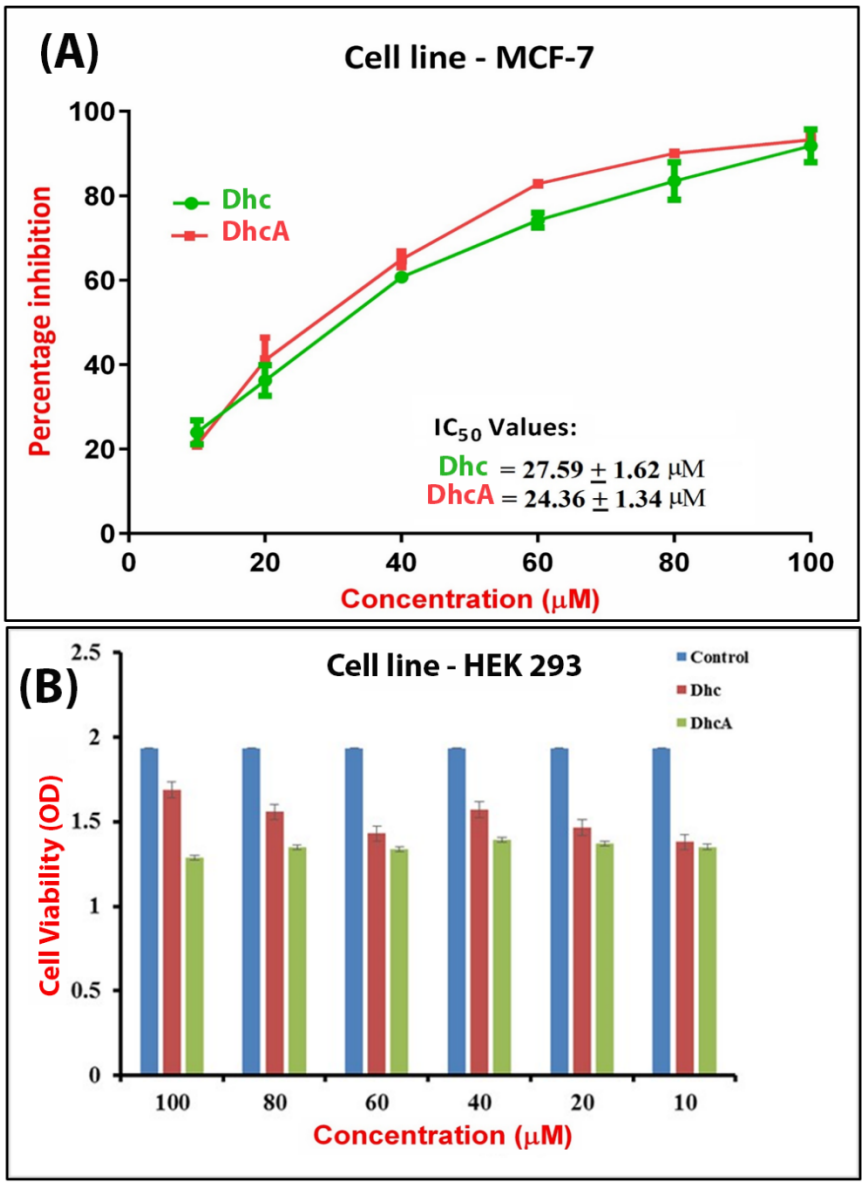

Figure 1. Cytotoxicity of Dhc (green) and DhcA (red) showing anti-cancer properties against breast cancer cells (MCF7) (A) Cell growth was measured by the MTT assay and the IC_{50} values were calculated for their percentage inhibition. (B) Cytotoxicity of Dhc (red) and DhcA (green) showing against normal human embryonic kidney cell line (HEK293).

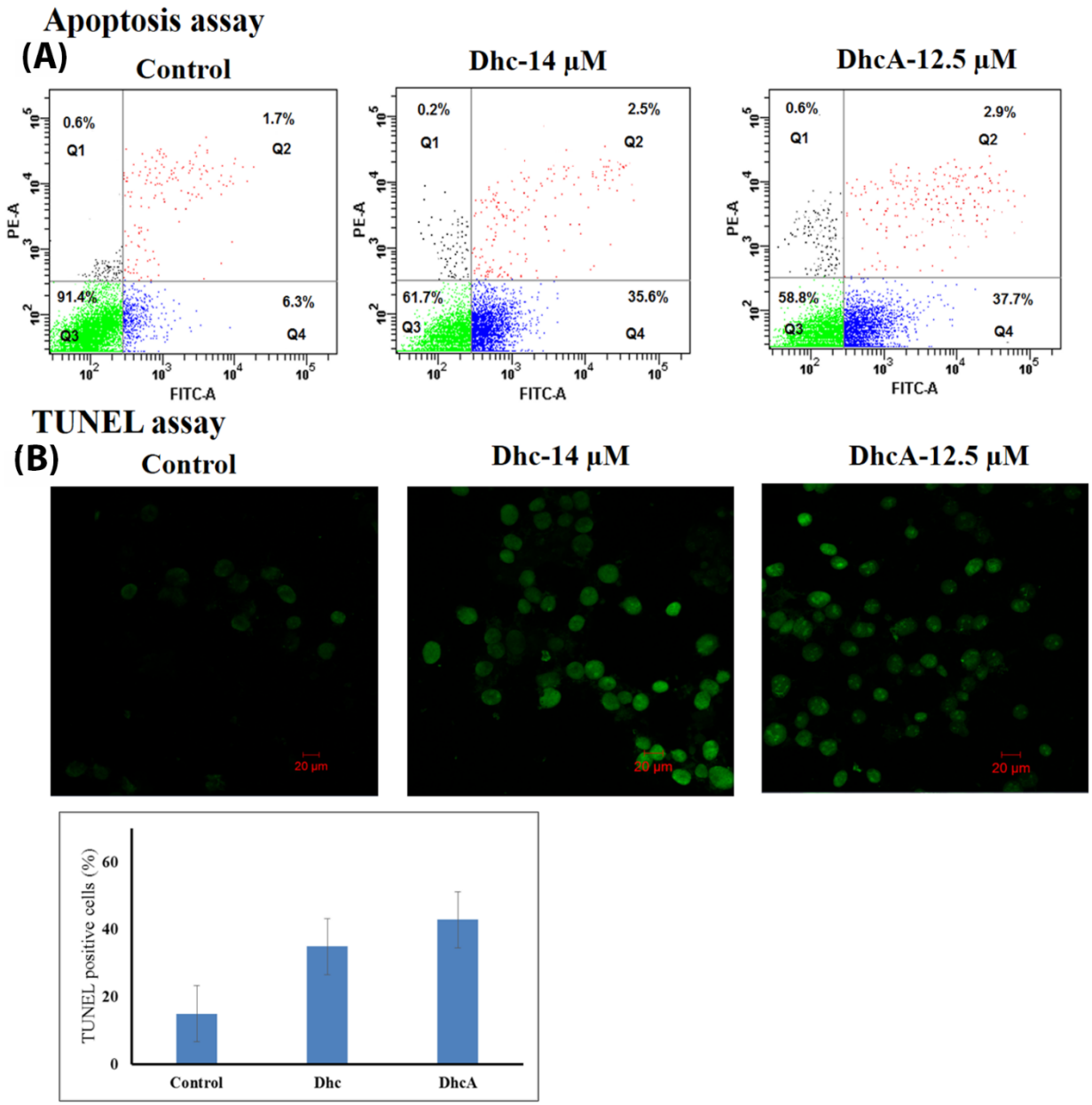

Figure 2. Effect of Dhc and DhcA on apoptosis of MCF-7 (A) Apoptotic cells were analyzed by flowcytometry after stained with Annexin V-FITC and PI. The percentage of cells are represented in quadrants. (B) Apoptosis was determined by terminal deoxynucleotidyl trans-ferase-mediated dUTPnick-end labelling (TUNEL). MCF-7 cells were cultured with 14 and 12.5 µM of Dhc and DhcA and without compound (Control) for 24 h. The percentage of apoptotic cell nuclei were given in the graph.

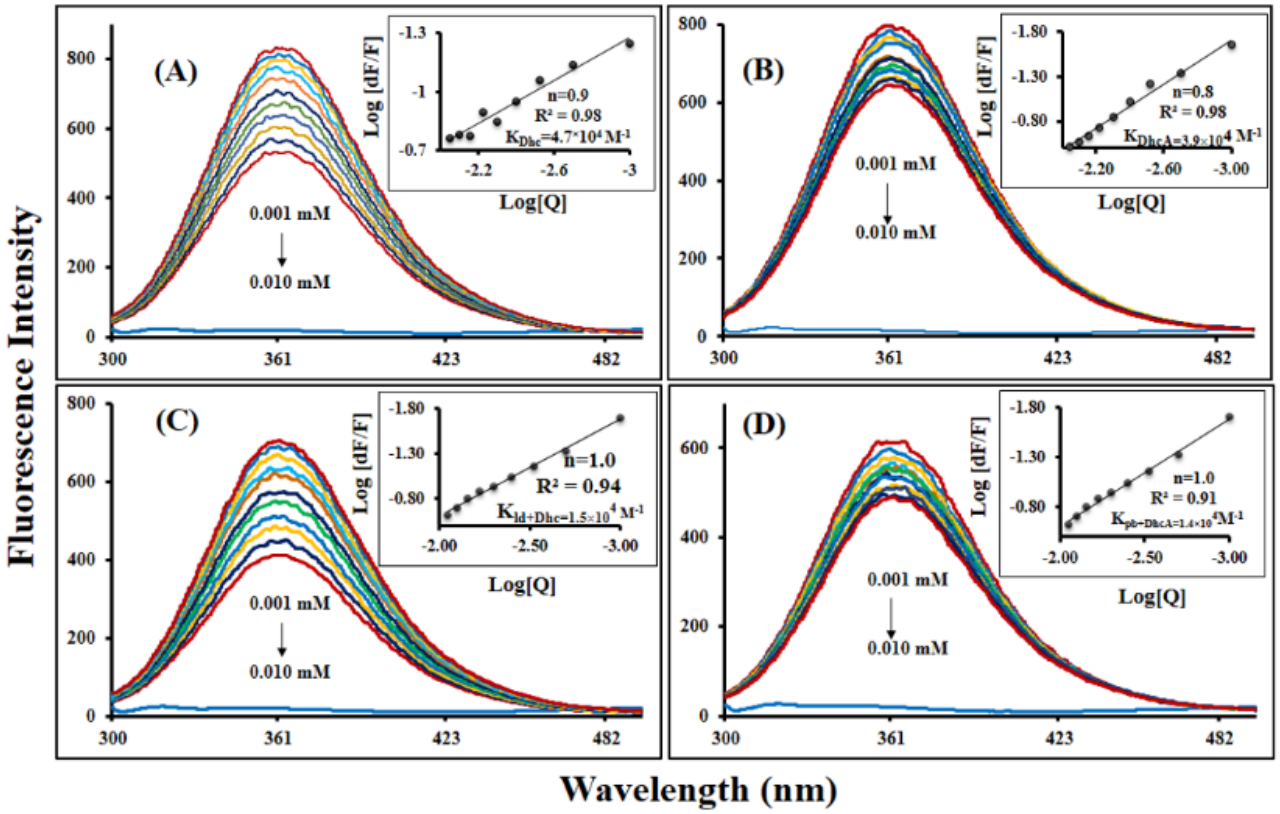

Figure 3. Fluorescence spectra of (A) Dhc–HSA (B) DhcA–HSA (C) lidocaine(ld)–Dhc–HSA (D) Phenylbutazone(pb)–DhcA–HSA. The concentrations of HSA was 0.001 mM, ld and pb were 0.01 mM, whereas the Dhc and DhcA concentrations were 0.001-0.010 mM, respectively at (λ_{ex} = 285 nm, T=296 K, pH 7.40).

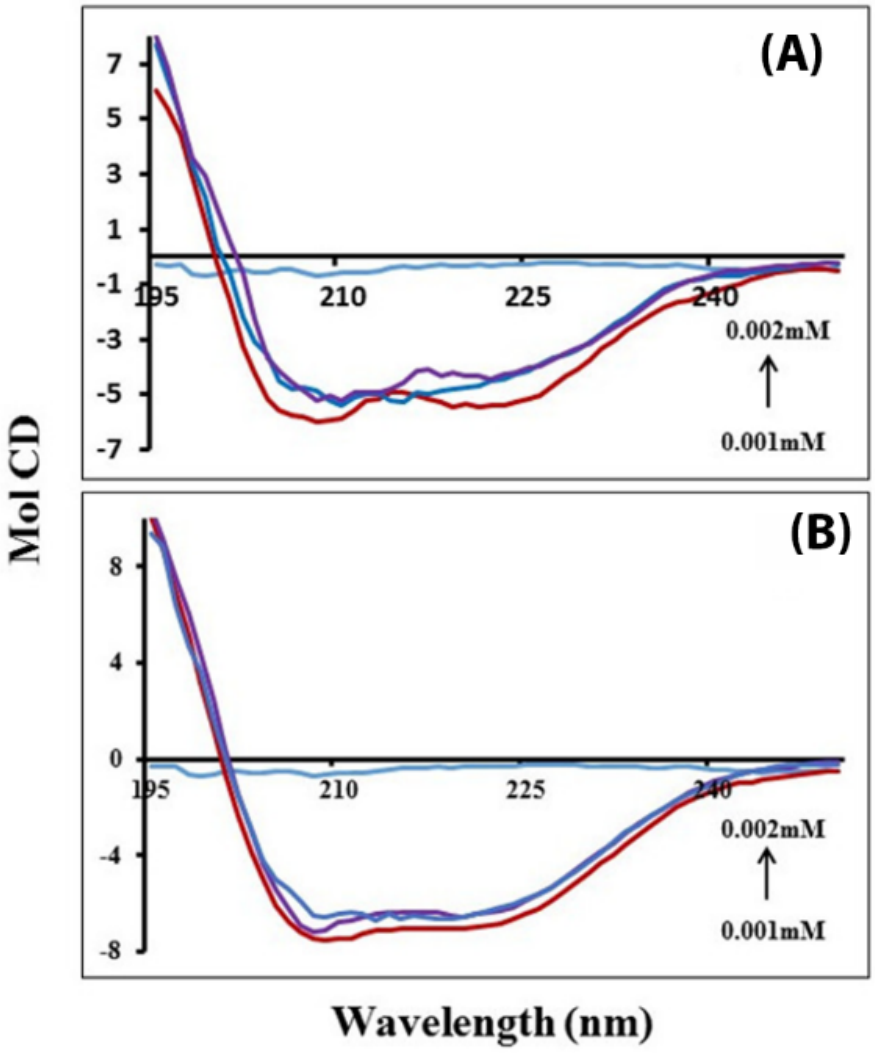

Figure 4. CD spectra of the (A) Dhc–HSA system (B) DhcA–HSA; difference in spectra due to concentrations of HSA (0.001 mM); Dhc and DhcA (0.001-0.002 mM) in the region of 195-250 nm.

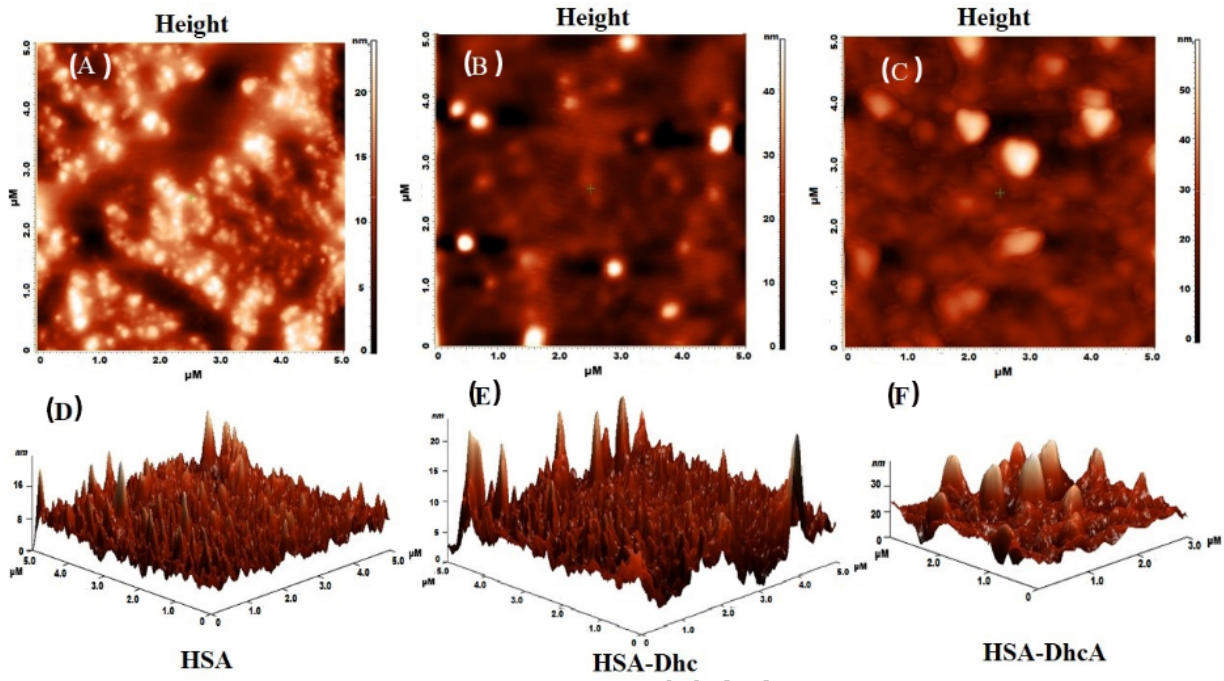

Figure 5. AFM topography images (A) free HSA (B) HSA–Dhc **(C)** HSA–DhcA. Height of the images given in 3D (D) free HSA (E) HSA–Dhc and (F) HSA–DhcA complex. Samples were adsorbed onto mica under tapping mode in a PBS buffer solution and the scan of the images is at 5 × 5 µm.

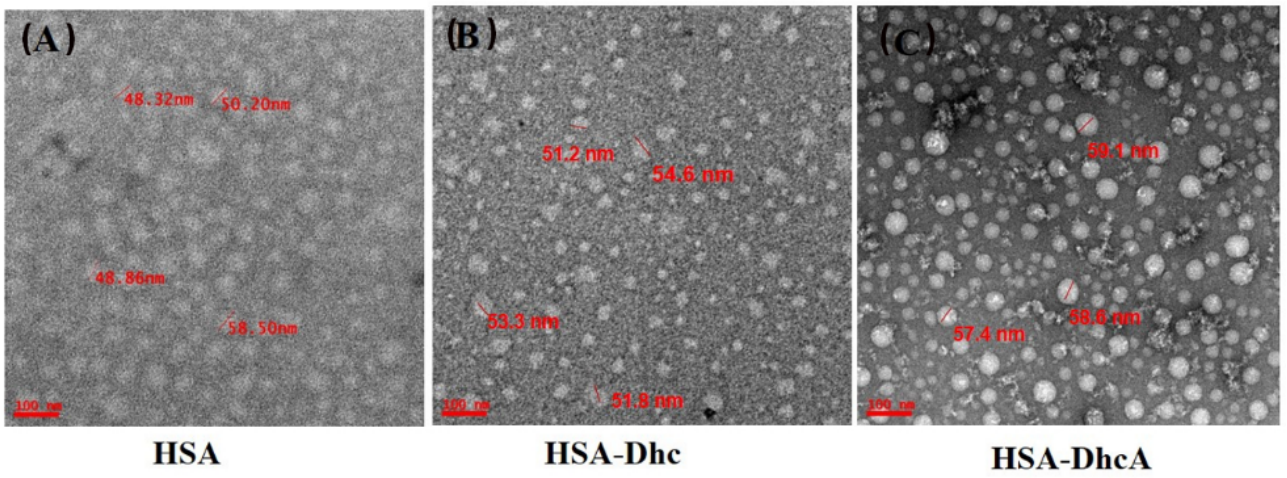

Figure 6. TEM micrographs of (A) free HSA (10µm) (B) HSA–Dhc (10µm-50µm) **(C)** HSA–DhcA complexes (10µm-50µm). Samples were adsorbed on copper grid and the scan of images is at 100 nm.

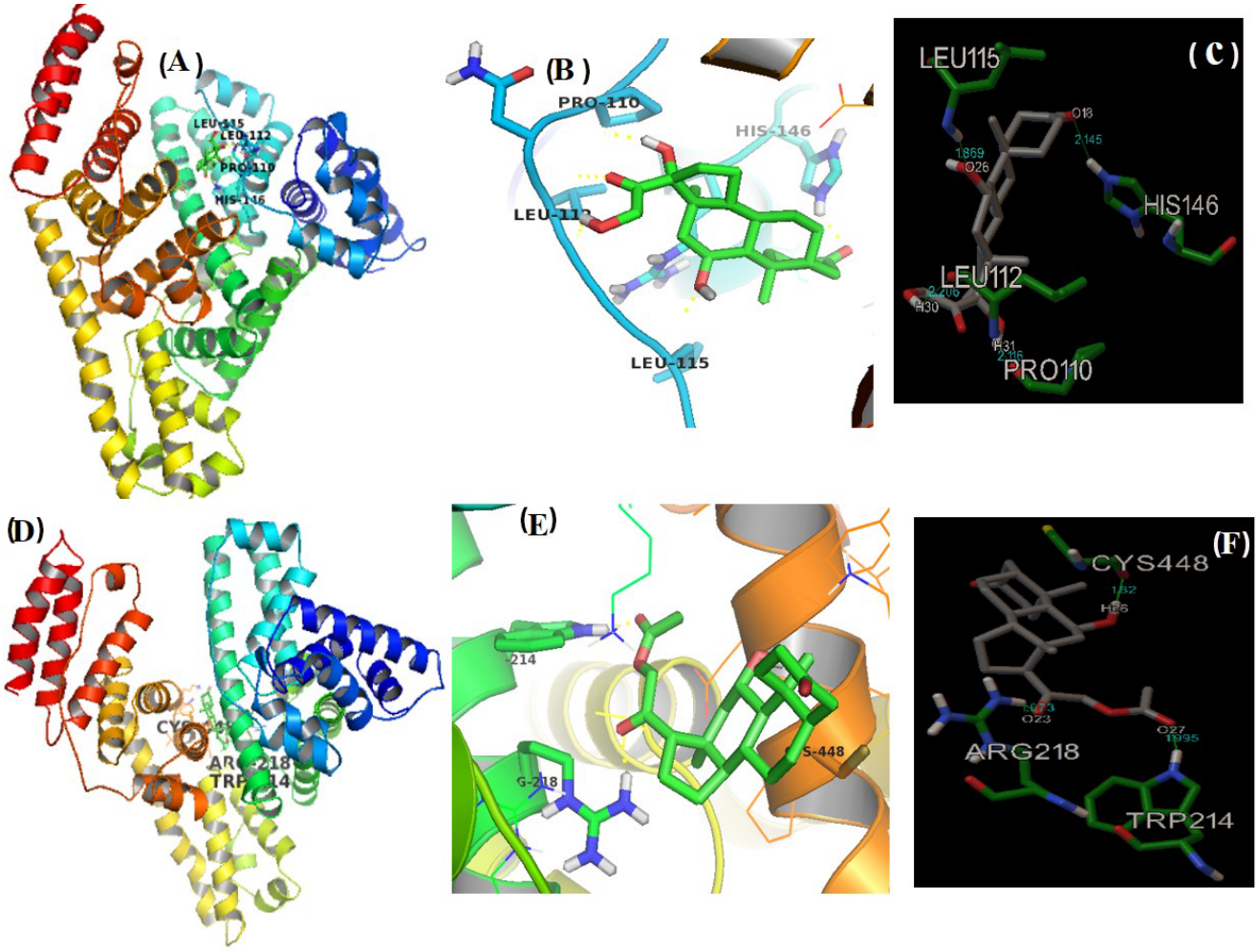

Figure 7. Cartoon representation of (A) and (D) HSA–Dhc and HSA–DhcA complexes and (B) and (E) Conformations of HSA after binding Dhc and DhcA (C) and (F) Hydrogen bonds and bond distance between HSA residues-Dhc and HSA residues-DhcA are represented by dashed lines.

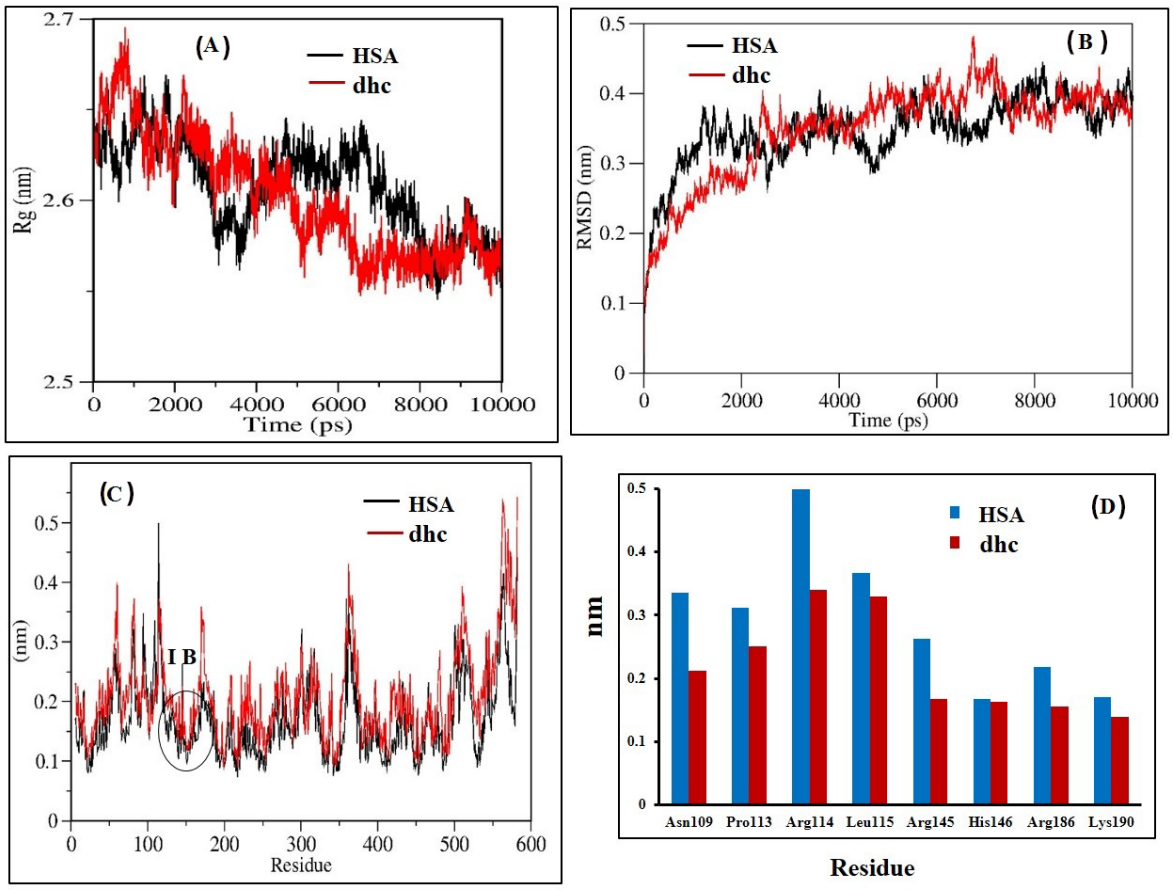

Figure 8. Radius of gyration of (A) free HSA (Black) and HSA–Dhc complex (Red) (B) Root-mean-square deviation (RMSD) for HSA–Dhc complex (C) Root-mean-square fluctuation of free HSA and HSA–Dhc complex (D) residues of free HSA and HSA–Dhc complex in the domain IB from MD simulation with respect to docking results as a function of the simulation time.

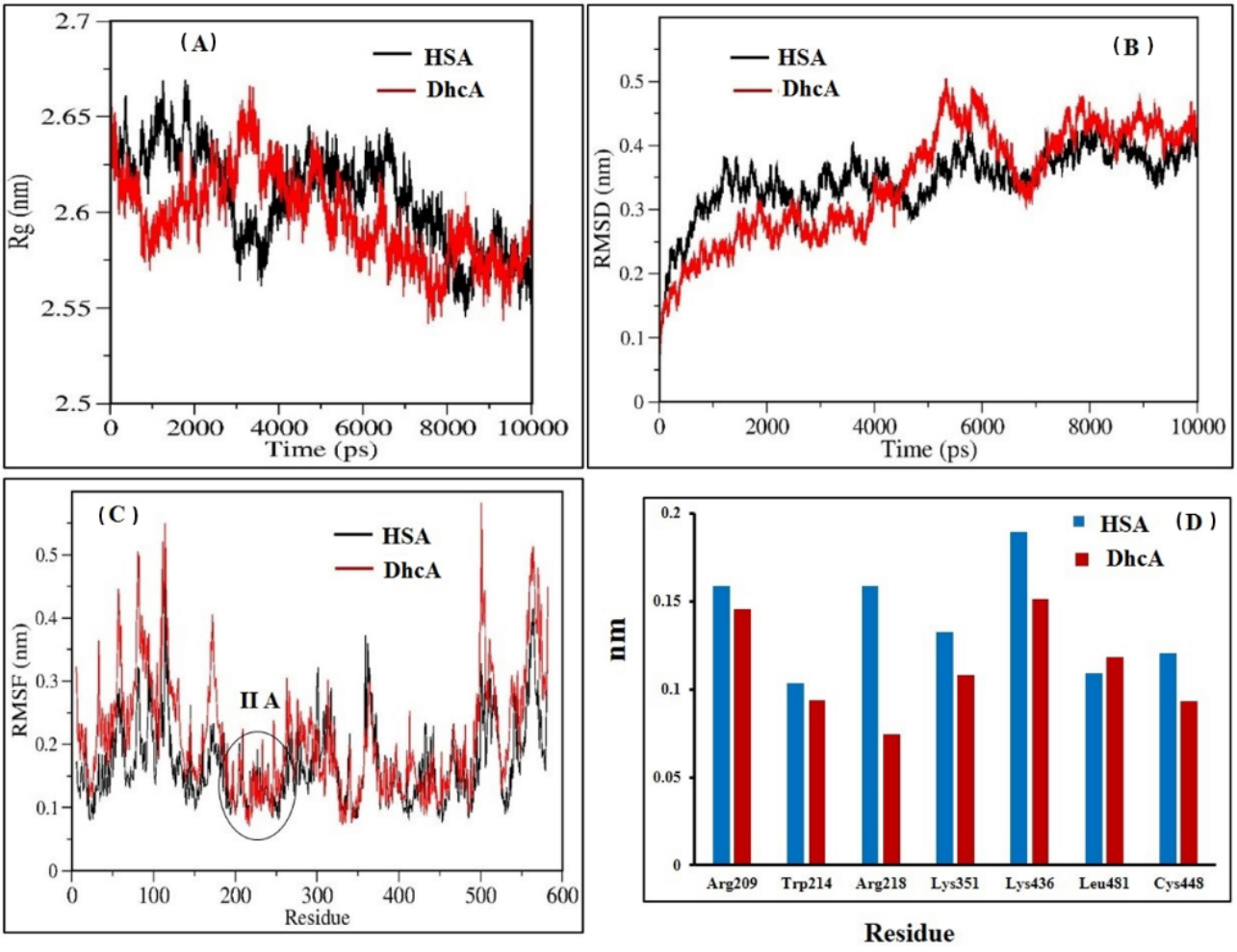

Figure 9. (A) Radius of gyration of free HSA (Black) and HSA–DhcA complex (red) (B) Root-mean-square deviation (RMSD) for HSA–DhcA complex (C) Root-mean-square fluctuation of free HSA and HSA–DhcA complex (D) residues of free HSA and HSA–DhcA complex in the domain IIA from MD simulation with respect to docking results as a function of the simulation time.

Table 1. The change in percentage of secondary structural elements of HSA upon addition of Dhc and DhcA.

	α-helix	**β-sheet**	**Random coil**
HSA (0.001 mM)	58.4±0.5	22.8±1.2	18.8±1.5
HSA–Dhc (0.001 mM)	58±0.3	21.2±0.8	20.8±1.4
HSA–Dhc (0.002 mM)	56.3±0.5	23.9±1.3	19.8±1.0
HSA–DhcA (0.001 mM)	56.28±0.8	25.6±1.5	21.22±0.9
HSA–DhcA (0.002 mM)	53±0.3	25.6±0.5	21.4±1.8

Spectroscopic evaluation of synthesized 5β-dihydrocortisol and 5β-dihydrocortisol acetate binding mechanism with human serum albumin and their role in anticancer activity

Monika Kallubai[a] , Srinivasa P Reddy[b] , Shreya Dubey[a] , Dhevalapally B Ramachary[b] & Rajagopal Subramanyam[a*]

[a] *Department of Plant Sciences, School of Life Sciences, University of Hyderabad, Hyderabad 500046, India*

[b] *Catalysis Laboratory, School of Chemistry, University of Hyderabad, Hyderabad 500046, India*

*Corresponding author

Rajagopal Subramanyam

Department of Plant Sciences

School of Life Sciences

University of Hyderabad 500 046 India

Tel: +91-40-23134572

Fax: +91-40-23010120

Email:srgsl@uohyd.ernet.in

Supplementary Figures

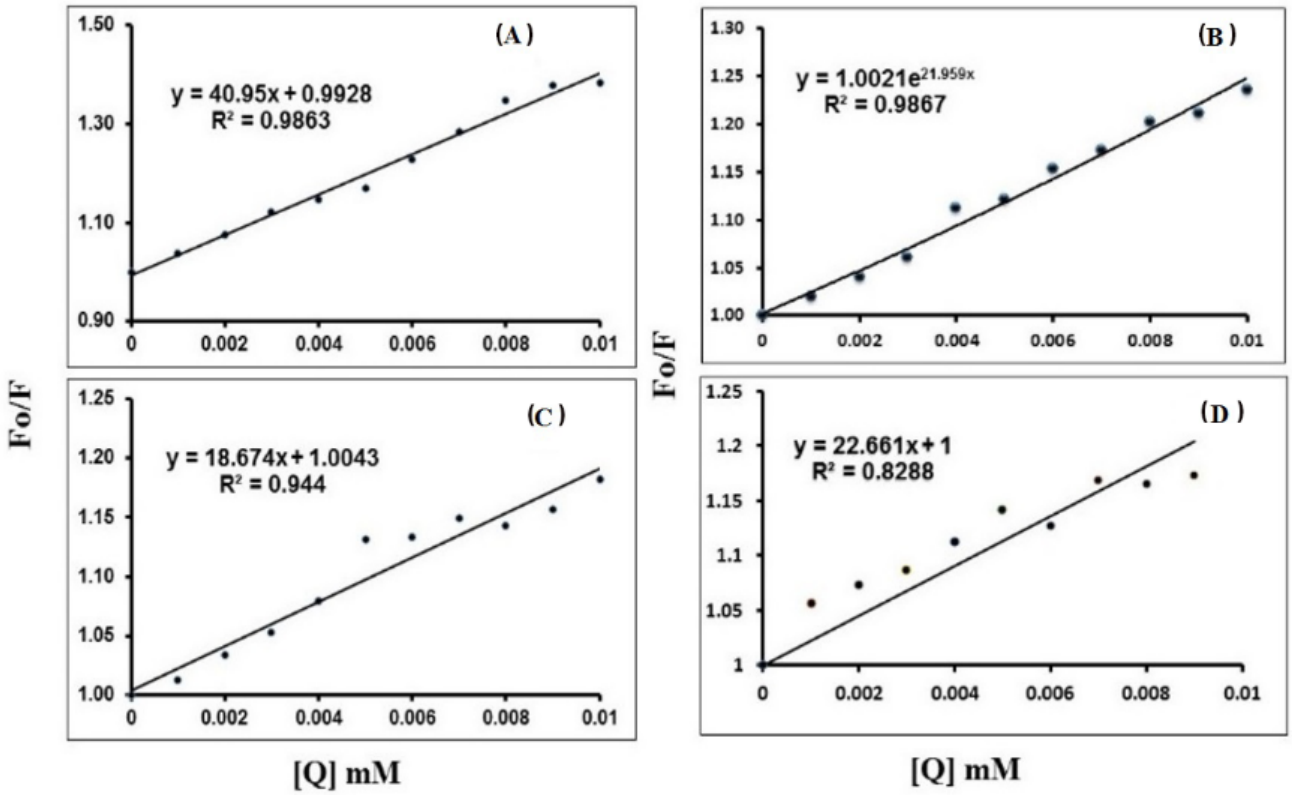

Supplementary Figure 1. Stern-Volmer plots of (A) HSA-Dhc complex (B) HSA-ld-Dhc complex (C) HSA-DhcA complex (D) HSA-pb-DhcA complex showing fluorescence quenching constant (kq) and plot of Fo/F against [Q] at λex = 285 nm and λem = 360 nm.

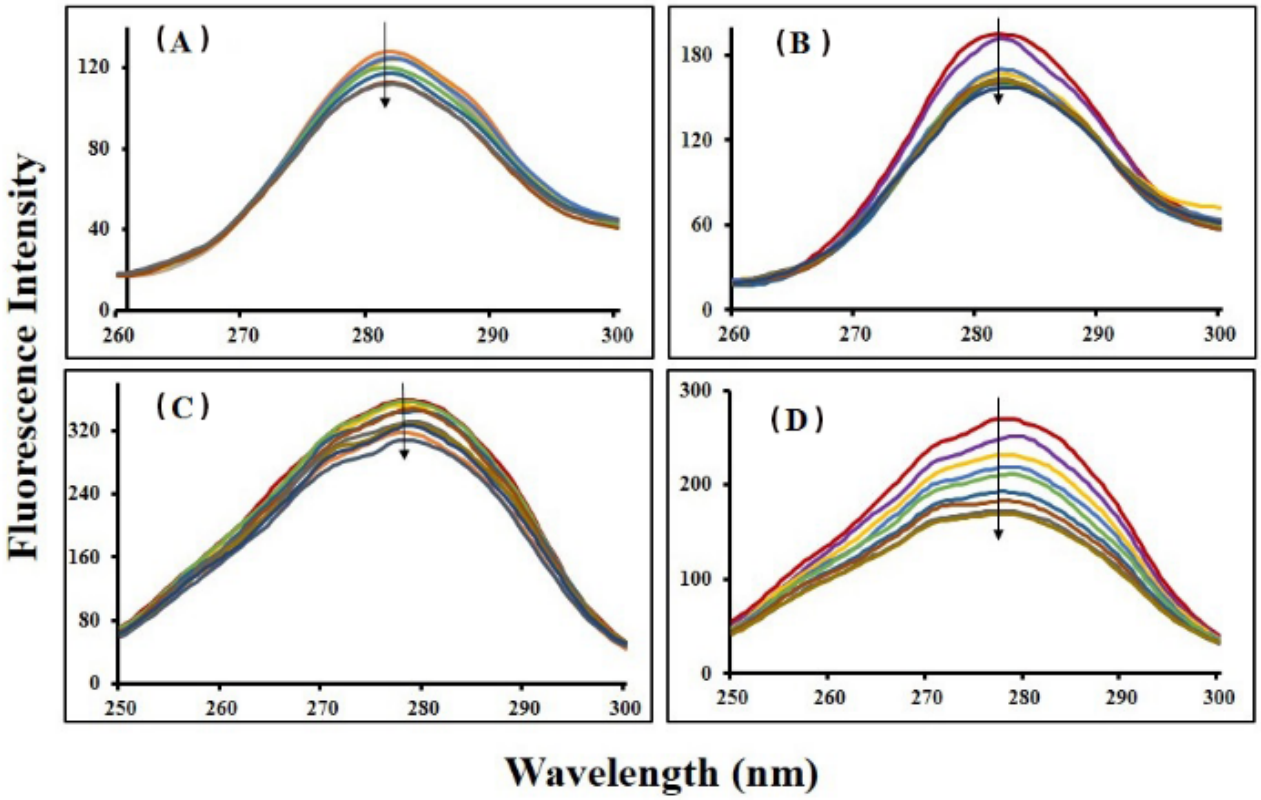

Supplementary Figure 2. Synchronous fluorescence spectra of (A) HSA-Dhc at Δ15 nm (B) HSA-DhcA at Δ15 nm (C) HSA-Dhc at Δ60 nm (D) HSA-DhcA at Δ60 nm. The concentrations of HSA was 0.001 mM, whereas the Dhc and DhcA concentrations were 0.001-0.010 mM, respectively at (λ_{ex} = 285 nm, T=296 K, pH 7.40).

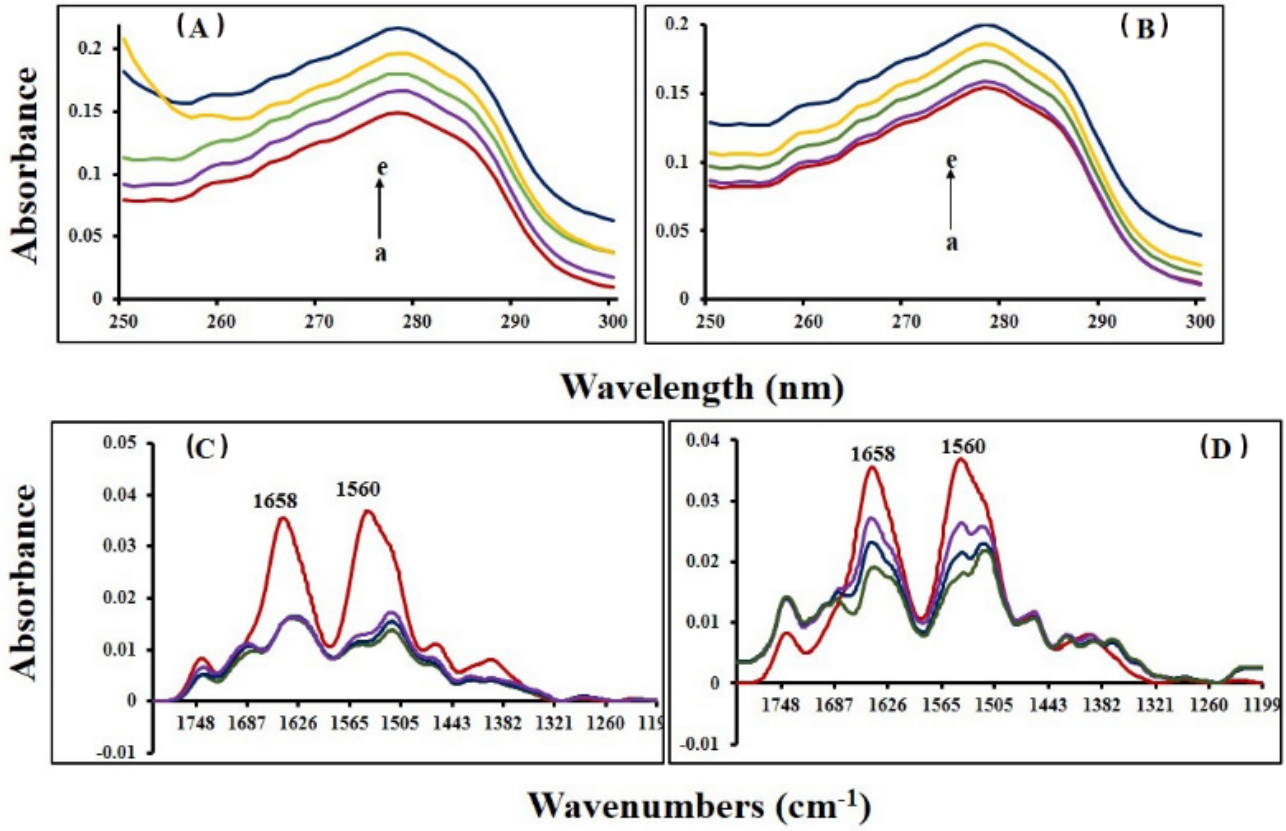

Supplementary Figure 3. The FT-IR spectra of (A) free HSA and difference in spectra after binding Dhc (HSA + Dhc solution) (B) free HSA and difference in spectra after binding DhcA in the region of 1800-1100 cm-1.